Electronic Supplementary Information (ESI) for:

Mechanistic Insights into Water-Stabilized Dye-Neurotransmitter Intermolecular Complexes in Zeolite Channels

Cristiano Invernizzi,[a] Laura M. Grimm,[b] Frank Biedermann,[b*] Ettore Fois,[a*] and Gloria Tabacchi[a*]

CONTENTS

S1. Computational details on models and methods

S1.1 Periodic models of zeolite L (ZL) and ZL-based host-guest systems

The host-guest materials object of the present study are based on zeolite L (ZL) as host (Fig. S1). This zeolite has framework type LTL, ideal unit cell stoichiometry $K_9Al_9Si_{27}O_{72}\cdot mH_2O$, and belongs to the space group *P6/mmm*. The primary building units are TO_4 tetrehedra (T=Si or Al). The framework can be considered as formed by cancrinite cages stacked along the *c* axis.[1,2] This arrangement generates 12-membered-ring (12MR) channels with approximately circular section and smaller 8-membered-ring (8MR) channels with elliptical section, whose axes are both parallel to the *c* axis. These channels are connected by a non-planar 8MR characterized by a boat-shape. As can be seen in Fig. S1, the parallel 12MR channels impose space confinement on guest molecules – *e.g.* water in the crystallographic structure of hydrated ZL. Such one-dimensional channel system is characterized by pore openings (0.71 nm) and maximum cage diameters (1.2 nm) which are comparable to the size of several neutral or positively charged organic chromophores. These structural features have made ZL a very useful host matrix for the confinement of photoactive guest species; in particular, very high concentrations of uniformly oriented chromophores, behaving similar to monomeric species, have been realized.[3]

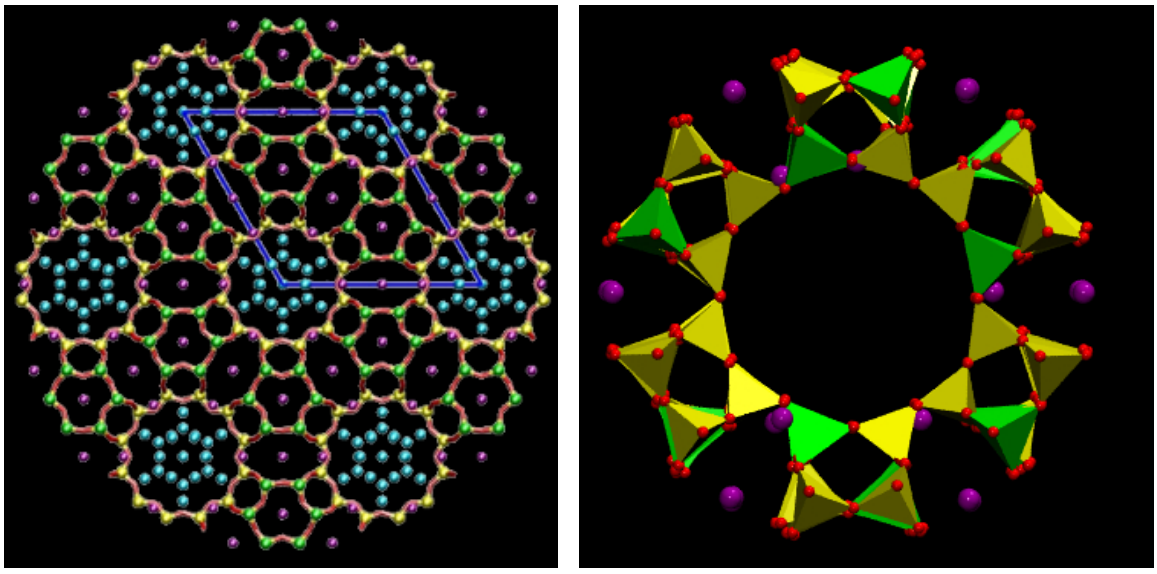

Fig. S1. Left panel: Crystal structure of hydrated zeolite L projected in the *ab* plane, showing the main channel, characterized by a twelve-membered ring (12MR), and containing the water molecules. The channel axis is parallel to *c*. The 6MR-cancrinite cages and the elliptical 8MR channels are also shown. The blue solid lines indicate the size of the unit cell. Right panel: Graphical representation of the section of a 12MR channel showing the 12 TO_4 (T=Al or Si) tetrahedral building units which define the pore opening (diameter: 0.71 nm). Color codes: green, yellow = Al/Si sites; red = framework oxygen sites; violet = K sites; cyan = water oxygen sites. Extraframework sites have fractional occupancy.

The fluorescent nanozeolite receptors described in ref.[4] contained the chromophore 2,7-dimethyldiazapyrenium (MDAP) as guest species in the channels of ZL nanocrystals, and were employed for the selective detection of the neurotransmitter serotonin (SERO) (see Scheme 1). The detection of SERO was reported to be due to the high-affinity binding of SERO with the nanosensor,[4] presumably caused by the formation of a MDAP+SERO intermolecular complex in the ZL channels.

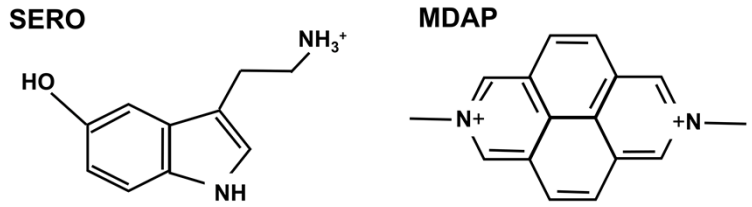

Scheme 1. Structural formulas of the neurotransmitter serotonin (SERO, charge: +1) and the chromophore 2,7-dimethyldiazapyrenium (MDAP, charge: +2)

In this work, three periodic models of ZL-based host-guest systems were investigated: (SERO)ZL, containing SERO as guest species; (MDAP)ZL, containing MDAP as guest species; (MDAP+SERO)ZL, containing the MDAP+SERO complex as guest species. All three models also contain water molecules in the ZL channels.

S1.2. AIMD simulations and geometry optimizations on periodic models

Host-guest inorganic-organic materials based on zeolite systems are crystalline materials, which are typically modelled by adopting periodic boundary conditions (PBC). Specifically, the material is modelled by replicating in the three dimensions the content of a simulation unit cell, which contains the coordinates of the zeolite framework and extraframework cations, the guest species, and the water molecules, which are normally co-present in zeolite pores in humid conditions.

Since structural crystallographic data on the three host-guest systems herein investigated - constituted by ZL as host, and SERO, MDAP, and the MDAP+SERO complex as guest species – were, to the best of our knowledge, not available in the literature, the initial guess structures of the simulation systems adopted in this study were built starting from the crystallographic data of ZL.

The ZL crystallographic unit cell is hexagonal, with cell parameters: $a = b = 18.466$ Å; $c = 7.476$ Å; $\beta = 120°$.[5] The framework stoichiometry is $Al_9Si_{27}O_{72}$. The crystallographic unit cell also contains 9 extraframework K^+ cations, which balance the negative charge of the 9 AlO_4 tetrahedra. The main channel axis is aligned to the *z* direction, i.e. to the *c* axis of the crystallographic unit cell.

The size of the simulation cell has been determined by considering the size of the largest guest species investigated in this work – namely, the MDAP+SERO supramolecular complex. In particular, a

simulation cell built by replicating 3 ZL crystallographic unit cells along *c* was found to be sufficient to accommodate MDAP+SERO. Special care was taken to check that the periodic images of the guest species were not in close contact.

Hence, in all the calculations of this work, the periodic crystal model for ZL consisted of three crystallographic unit cells along the channel axis (a=b=18.466 Å; c=3×7.476 Å; β=120°). This ZL model would correspond to a simulation cell stoichiometry of $K_{27}[Al_{27}Si_{81}O_{216}]$, since 27 monovalent extraframework cations are needed to balance the total negative charge of the ZL framework, due to the 27 AlO_4 tetrahedra.

In the model systems presented herein, a number of K^+ cations ranging from 1 to 3 was removed in order to incorporate the charged host species (SERO and/or MDAP) in the ZL main channel. The eliminated K^+ cations were originally located in positions close to the 12MR channel.

Specifically, the ZL composition per simulation cell in the three considered models was:

1) $K_{26}[Al_{27}Si_{81}O_{216}]$ for (SERO)ZL, containing SERO and 46 water molecules (total number of atoms in the simulation cell: 514).
2) $K_{25}[Al_{27}Si_{81}O_{216}]$ for (MDAP)ZL, containing MDAP and 44 water molecules (total number of atoms in the simulation cell: 513), and
3) $K_{24}[Al_{27}Si_{81}O_{216}]$ for (MDAP+SERO)ZL, containing the MDAP+SERO complex and 37 water molecules (total number of atoms in the simulation cell: 517);

Such stoichiometries were determined as follows.

In the (SERO)ZL model (guest species: SERO, charge: +1), only one K^+ had to be removed to accommodate SERO, while in (MDAP)ZL (guest species: MDAP, charge: +2), two K^+ were replaced by one MDAP. The water content of (SERO)ZL and (MDAP)ZL amounted to 15.33 and 14.67 H_2Os per crystallographic unit cell, respectively, and all the H_2Os were inside the main ZL channel.

Following the same reasoning, the guest species in the (MDAP+SERO)ZL model bear a total positive charge of +3. Consequently, three K^+ had to be removed in order to insert MDAP and SERO while maintaining electroneutrality. The ZL stoichiometry per simulation cell was $K_{24}[Al_{27}Si_{81}O_{216}]$. The water content corresponds to 12.33 H_2O molecules per crystallographic unit cell, and all the 37 H_2Os were located inside the ZL 12MR channel.

The three above-mentioned periodic models are graphically represented in Fig. S2.

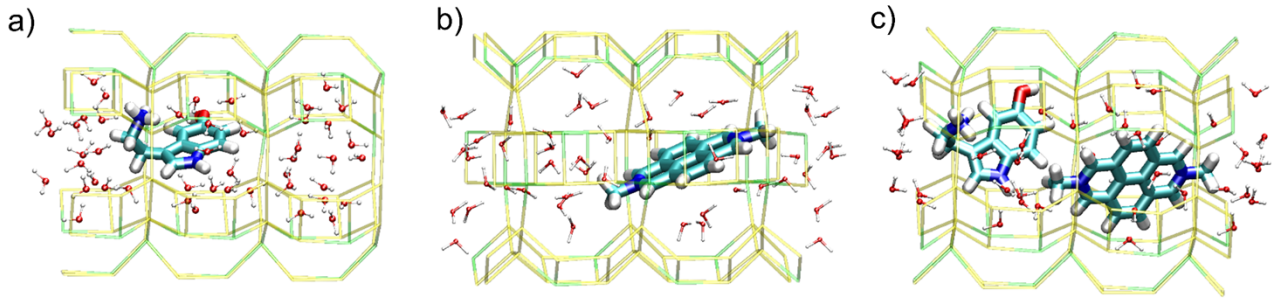

Fig. S2. Graphical representation of the simulation cell of periodic models: **a)** (SERO)ZL; **b)** (MDAP)ZL; **c)** (MDAP+SERO)ZL. In each case, the depicted configuration corresponds to the minimum energy structure calculated for each model. Color codes: yellow = Si; green = Al; red = O; cyan = C; blue = N; white=H. Framework oxygen atoms and extraframework K^+ cations are not shown for clarity.

The number of water molecules to be included in each model was determined by starting from the water molecules present in the hydrated ZL host. In particular, 18 H_2Os are contained in the crystallographic unit cell of hydrated ZL,[6] hence the hydrated ZL simulation cell (formed by 3 crystallographic unit cells) should contain 54 H_2Os. However, the number of H_2O in the three models is lower than 54 because some H_2Os must be removed in order to accomodate MDAP and SERO.

Specifically, the number of H_2Os in (SERO)ZL and (MDAP)ZL (46 and 44, respectively) was established by subtracting to the total volume of the water molecules in the simulation cell of hydrated ZL the molecular volume of MDAP and SERO, respectively. Similarly, the number of water molecules in (MDAP+SERO)ZL was determined by subtracting to the total H_2O volume in hydrated ZL the sum of the molecular volumes of MDAP and SERO. All molecular volumes were calculated with the Gaussian 09 code.[7] Once determined, for each model, the number of water molecules to be removed, we chose to eliminate the H_2Os which overlapped with the guest species and/or were at less than van der Waals distance from the guests.

In the guess structure of all the considered models, the main molecular axis of the guest species was aligned with the ZL main channel axis (*z* direction).

For all models, both minimum energy structures (0 K) and structures sampled from the AIMD simulations of the investigated systems at room temperature (298 K) were considered.

In all the performed calculations, conducted with PBC, the PBE[8] approximation to Density Functional Theory (DFT), combined with empirical dispersion corrections[9], was employed. Wavefunctions were expanded in planewaves (PW), at the Γ point of the Brillouin zone. The PW basis size was defined by the cutoff imposed for the wavefunctions and for the electronic density (25 Ry and 200 Ry, respectively). The interactions of electrons with the cores has been treated by using ultrasoft

pseudopotentials of the Vanderbilt type for the N, O, C, H atoms,[10,11] while norm conserving pseudopotentials with non-linear core corrections have been employed for Si, Al, and K.[12–14]

Importantly, no symmetry constraints were imposed to the atomic positions during the calculations, only the simulation cell parameters (with periodic boundary conditions) were kept fixed at the experimental values.

All the AIMD simulations were performed in the framework of the NVT ensemble, by using the Nose-Hoover chain thermostats.[15,16] The Car-Parrinello equations of motion[17,18] were integrated with a time step of 5 atomic units (a.u.) (0.121 fs) and a fictitious mass of the wavefunction's coefficients of 500 a.u. The target temperature was set to 298 K. For all the three models, 5 ps equilibration AIMD were carried out. The total elapsed times for the production AIMD runs were 36.32 ps, 42.35 ps and 35.09 ps for (SERO)ZL, (MDAP)ZL and (MDAP+SERO)ZL, respectively.

Minimum energy structures of the three models were obtained by performing structural optimizations of different configurations sampled along the pertaining AIMD trajectories and choosing the resulting lowest-energy one. The convergence criterion for geometry optimizations required a maximum force on the ions below 1×10^{-4} Hartree/Bohr.[18]

All the calculations on the periodic models were performed with the CPMD code.[19]

S1.3. Calculations on isolated MDAP and SERO in vacuum

To aid assignment of the electronic excitation bands in the simulated UV-vis spectra of the MDAP+SERO complex in ZL, calculations on the isolated MDAP and SERO species in vacuum were performed. The geometries of both molecules were optimized using the ωB97XD functional,[20] which takes into account van der Waals interaction in an empirical approach, at the ωB97XD/6-311G(d,p) level. The electronic excitation calculations were performed at the TD-DFT/CAM-B3LYP/6-311++G(df,pd) level. For both MDAP and SERO, the first 20 excitations were considered.

To validate the choice of the TD-DFT/CAM-B3LYP/6-311++G(df,pd) approach, the isolated MDAP geometry in vacuum was re-optimized at the MP2/6-311++G(df,pd) level, and the electronic excitations were computed using different theory levels. Specifically, the electronic excitations calculated at the TD-DFT/CAM-B3LYP/6-311++G(df,pd) level were compared with those obtained using TD-DFT in conjunction with the PBE0[21] hybrid functional (TD-DFT/PBE0/6-311++G(df,pd)), and, finally, with a higher level quantum-mechanical (QM) post-Hartree-Fock approach, namely the Equation Of Motion – Coupled Cluster with Single and Double excitations (EOM-CCSD).[22,23] By

using the three above-mentioned methods, we calculated the wavelengths (λ_1, λ_2) and the oscillator strengths (f_1, f_2) of the two lowest-energy excitations of isolated MDAP in vacuum. The results of such tests are reported in Table S1.

Level of Theory	λ_1	λ_2	f_1	f_2
EOM-CCSD/6-311++G(df,pd)	350.07	277.27	0.1294	0.2457
TD-DFT/CAM-B3LYP/6-311++G(df,pd)	355.85	305.43	0.1337	0.2625
TD-DFT/PBE0/6-311++G(df,pd)	374.03	323.57	0.1091	0.2243

Table S1. Wavelength λ (nm) and oscillator strength f for the two lowest-energy excitations calculated for isolated MDAP in vacuum at different theory levels.

From the reported data, it emerges that, within the TD-DFT framework, the CAM-B3LYP functional can reproduce the EOM-CCSD values obtained for the first two excitations of MDAP better than the PBE0 functional. Moreover, it has been reported that the average best agreement with EOM-CCSD is provided by CAM-B3LYP, even in the case of charge-transfer transitions.[24] For this reason, we employed the TD-DFT/CAM-B3LYP/6-311++G(df,pd) scheme for the calculation of the electronic excitations of the target guest species throughout this work.

For all the electronic excitation calculations, the GAUSSIAN 09 code was used.[7]

S1.4. Calculation of the electronic excitation spectra on cluster models

AIMD simulations based on pure DFT approximations on periodic models have shown to be a useful tool to predict the structural properties of ZL-based host-guest systems at room temperature conditions, thus enabling comparison with experiments and facilitating the interpretation of available experimental data. On the other hand, the calculation of electronic excitation properties – in particular, the simulation of UV-vis spectra of the incorporated photoactive species – requires methodologies characterized by an accuracy level superior to pure DFT approaches. Usually, time-dependent DFT (TD-DFT)[25] with hybrid DFT approximation and extended (triple-zeta) basis sets offer a convenient accuracy vs. computational cost balance. For this reason, we used cluster models to investigate the optical properties of the host-guest systems described in this work, and in particular to reproduce the electronic spectra of the incorporated species.

Specifically, the electronic excitation spectra of the investigated systems were calculated by TD-DFT using the CAM-B3LYP[26] range-separated hybrid functional and the 6-311++G(df,pd) basis set on the cluster models shown in Fig. S3. These cluster models were extracted from the minimum energy structure of the periodic models (SERO)ZL, (MDAP)ZL, and (MDAP+SERO)ZL.

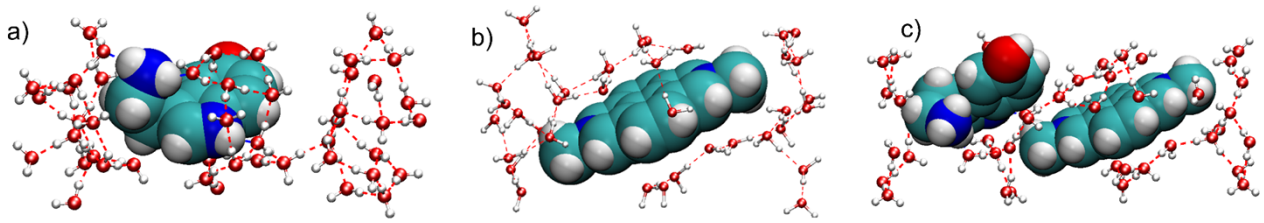

Fig. S3 a-c): Cluster models used to calculate electronic excitation spectra. Atom coordinates were extracted from the periodic minimum energy structure of: a) (SERO)ZL; b) (MDAP)ZL; c) (MDAP+SERO)ZL. The MDAP and SERO molecules (large spheres) were treated at the CAM-B3LYP/6-311++G(df,pd) level (QM), while H_2Os (ball-and-stick) were treated as point charges (MM) with the RESP[27] charges. Color codes: red = O; cyan = C; blue = N; white=H, red dashed lines: hydrogen bonds.

To limit computational costs, while MDAP and SERO were treated at the CAM-B3LYP/6-311++G(df,pd) level, the water molecules were represented as point charges - *i.e.,* using a "molecular mechanics" (MM) treatment. Specifically, RESP (Restrained Electrostatic Potential)[27] charges were used, assigning charges of +0.34195 and -0.6839 to the H and O atoms of water, respectively.

The same theoretical scheme was employed to calculate the electronic excitation spectra of MDAP and MDAP+SERO as thermal averages. In this case, the TD-DFT electronic excitations were computed on similar cluster models – constituted by the organic guests and the surrounding water molecules -, which were extracted from a set of 15 and 25 uncorrelated configurations sampled along the AIMD trajectories of (MDAP)ZL and (MDAP+SERO)ZL, respectively. This strategy allowed us to obtain thermally-averaged electronic excitation spectra which could be directly compared with the experimental UV-Vis spectra reported in Ref.[4]. Additionally, microscopic-level information could be gathered on possible factors affecting the position and the intensity of the bands in the experimental UV-Vis spectra[4] of the MDAP+SERO complex in ZL. The procedure adopted to calculate thermally averaged theoretical UV-Vis spectra is described below.

The configurations were randomly selected from the pertaining AIMD trajectories. Then, for each configuration, we extracted the coordinates of the guest organic species (i.e., MDAP and MDAP+SERO) and of the nearest water molecules (43 and 41 for (MDAP)ZL and (MDAP+SERO)ZL, respectively), including periodic images where needed in order to fully solvate the organic guests. The thermally-averaged UV-Vis spectra for the MDAP receptor and the MDAP+SERO complex were obtained by averaging over the electronic excitations computed for all the configurations sampled from the pertaining AIMD trajectories (15 and 25 configurations, respectively). Representative cluster models used to calculate the thermally averaged UV-vis spectrum of the MDAP+SERO complex are shown in Fig. 3c-f in the main text.

.

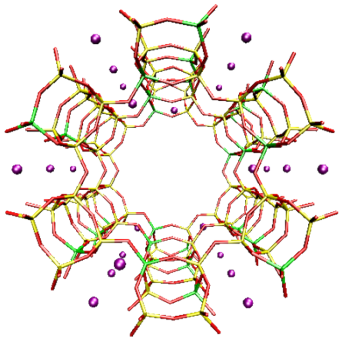

Fig. S4. Representation of the ZL channel used to build the cluster models for calculating Uv-Vis spectra from (MDAP)ZL and (MDAP+SERO)ZL optimized geometries. Yellow = Si; green = Al red = O; purple=K.

It would be of interest to evaluate also the effect of the zeolite framework structure on the electronic spectra. This insight was achieved by calculating the electronic excitation spectrum by including the surrounding ZL atoms, treated as point charges. In particular, a slice of the 12MR channel (see Fig. S4) containing the organic species and the solvating water molecules was selected, along with the pertaining extraframework K^+. The adopted zeolite atomic charges were taken from literature data,[28] while for the H_2O atoms RESP charges were adopted. In order to maintain electroneutrality, the dangling (external) O atoms of the ZL framework were capped with H atoms. A graphical representation of the cluster model for (MDAP+SERO)ZL is shown in Fig. S5. As can be seen, the ZL atoms included in the model fully surround the guest systems. An analogous cluster model was built in the case of (MDAP)ZL. For both systems, the electronic excitation calculation was performed by extracting the clusters from the (MDAP)ZL and (MDAP+SERO)ZL minimum energy geometries.

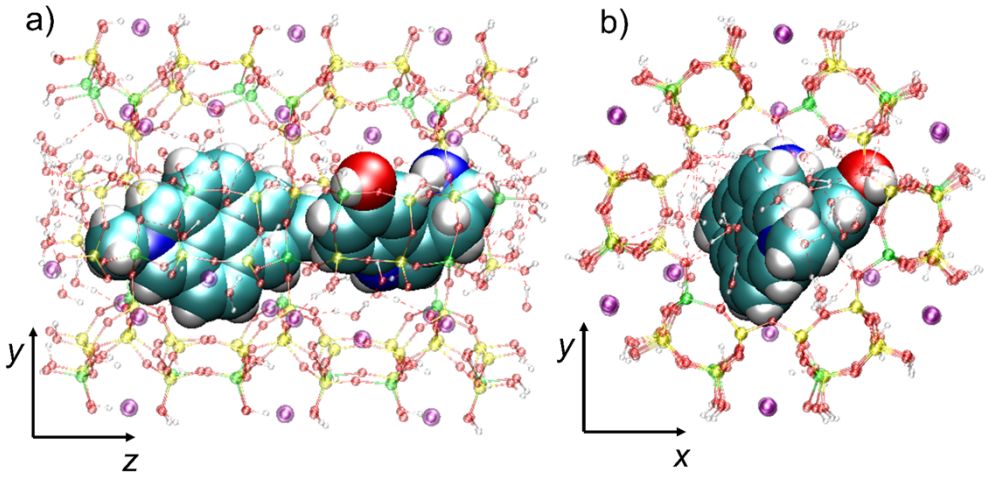

Fig. S5. Graphical representation in two different orientations a), b) of the cluster model used to calculate the UV-vis spectra for the minimum energy structure of (MDAP+SERO)ZL with the ZL environment. The coordinates were extracted from the minimum energy structure shown in Fig. S2c. The MDAP and SERO molecules (large sphere representation) were treated at the CAM-B3LYP/6-311++G(df,pd) level (QM), the water molecules were treated as RESP point charges, while point charges for ZL atoms and capping H were taken from Ref.[28]. Color codes: yellow = Si; green = Al; purple=K; red = O; cyan = C; blue = N; white=H.

S2. The minimum energy structure of the MDAP+SERO complex in ZL

In the minimum energy structure of (MDAP+SERO)ZL (Fig. S6) the aromatic part of SERO and MDAP maintains the typical nearly-planar geometry of π-conjugated systems. These moieties form an intermolecular complex, although they are not directly connected to each other via short-range interactions. The closest distance between the N atoms of MDAP and the aromatic C atoms of SERO is 5.621 Å, while the shortest intermolecular distance is 3.200 Å, indicating that the separation between these two charged moieties in ZL is sizeable. This result can be rationalized by recalling that both MDAP and SERO are positively charged (+2 and +1, respectively). Importantly, beside the negative charge of the ZL framework, and the confinement effect of the ZL channel (which is effective only in the *xy* plane, but not along *z*), intermolecular interactions involving water molecules cause MDAP and SERO to stay close to each other, despite their strongly repulsive Coulomb interactions. Indeed, four water molecules are located between MDAP and SERO (Fig. S6b), thus partially screening the repulsive interaction between the two positively charged guests.

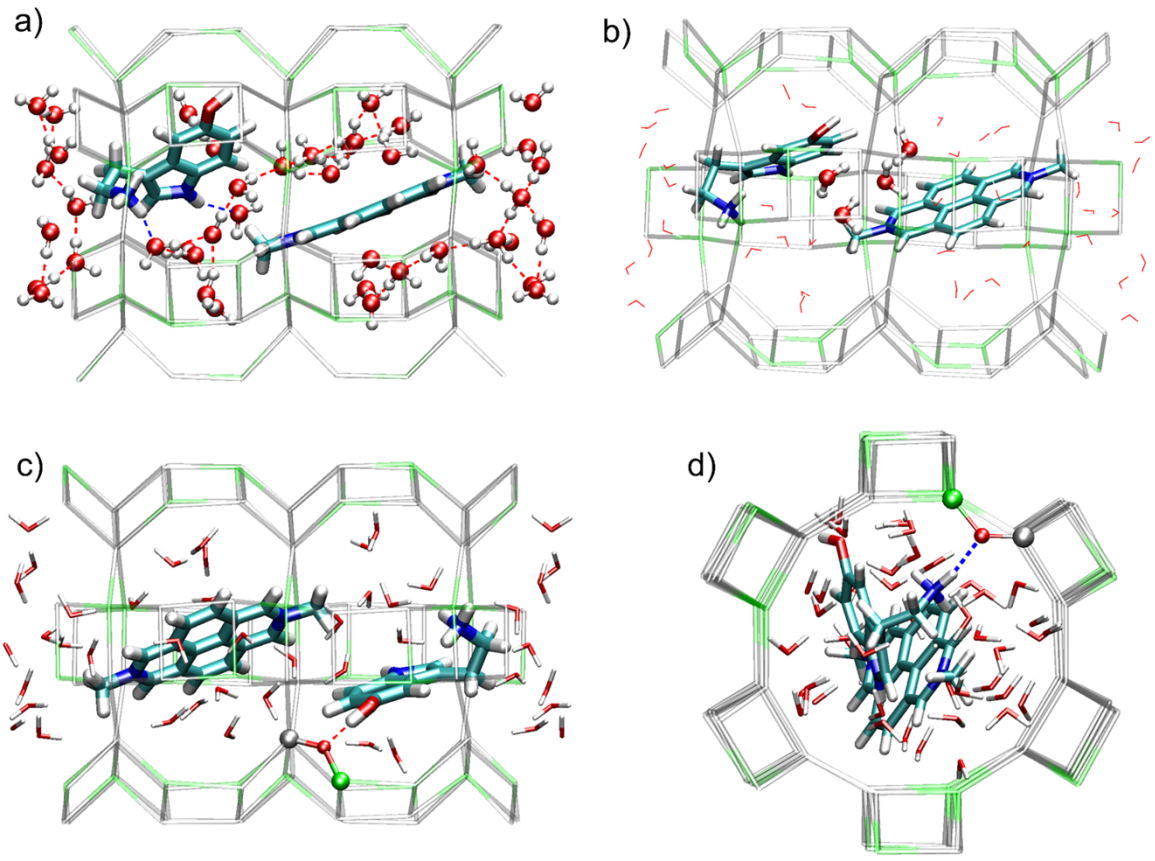

Fig. S6. Minimum energy structure of the (MDAP+SERO)ZL system in four different orientations evidencing: a) the MDAP+SERO complex and the surrounding water molecules; b) the four water molecules (in ball-and-stick) located between the two positively charged MDAP and SERO guests; c) the H-bond between SERO –OH group and a ZL framework oxygen (in ball-and-stick; d) the H-bond between SERO $–NH_3$ group and a ZL framework oxygen (in ball-and-stick r). Color codes: grey=Si; green=Al; red=O; blue=N; cyan=C; white=H. H-bonds are represented as dotted lines. Framework oxygens and extraframework K^+ are not shown for clarity.

Hence, even zeolitic water molecules play a key role in stabilizing such an unusual supramolecular system, acting as a sort of dielectric buffer between the two positively charged moieties. This complex interplay between effects of geometric confinement and intermolecular interactions allows for the formation of such a triply-positively charged MDAP+SERO complex.

While the MDAP molecule is located approximately in the middle of the ZL 12MR channel, with its axis oriented at about 30° with respect to the ZL channel axis, SERO is positioned close to the pore walls, with its molecular axis forming a 10° angle with the ZL channel axis. Notably, the SERO hydroxyl proton forms a strong hydrogen bond with a framework oxygen of an AlO_4 unit, its distance being 1.731 Å (Fig. S6c). Moreover, the $–NH_3$ group of SERO is strongly connected via hydrogen bonding interactions to the ZL framework (Fig. S6d). Specifically, two $–NH_3$ protons are at hydrogen bonding distance from two framework oxygens (1.790 Å and 1.913 Å), and the shorter distance refers to a framework oxygen belonging to an AlO_4 tetrahedron (Fig. S6d).

S3. Electronic excitations for isolated SERO and MDAP species

S3.1 SERO

As a neutral molecule, serotonin can have a large number of different conformational isomers, due to the possibility of reorienting both the –OH group and the ethylamine lateral chain, characterized by an inherent flexibility.[29] In this study, serotonin has been modeled in its protonated form (see Scheme 1), - *i.e.*, as reported in the nanozeolite receptor experiments described in Ref.[4] Therefore, a conformational search has been performed on the SERO protonated form at the ωB97XD/6-311G(d,p) level. The geometries of the four most stable conformers, along with their relative energy differences in kcal/mol, are shown in Fig. S7. The minimum energy structure features the OH group in an outward orientation, and the ethylamine chain pointing towards the aromatic part of the molecule, which is approximately planar.

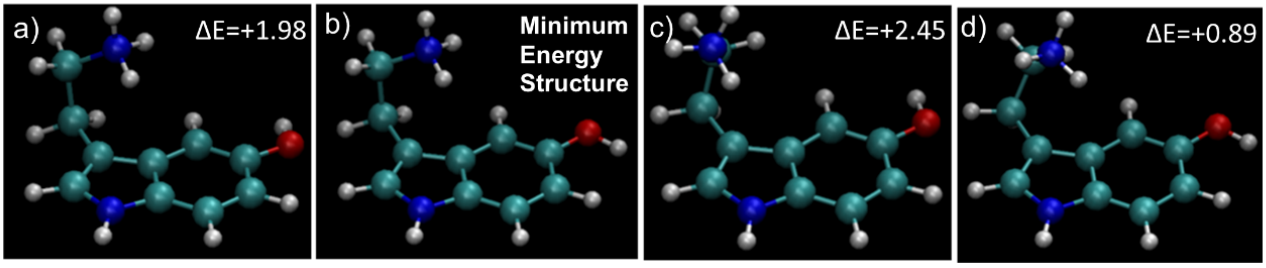

Fig. S7. The four most stable conformers found for isolated SERO. Energy differences (in kcal/mol) with respect to the minimum energy structure (panel b)) are also reported. Color codes as in Fig. S3.

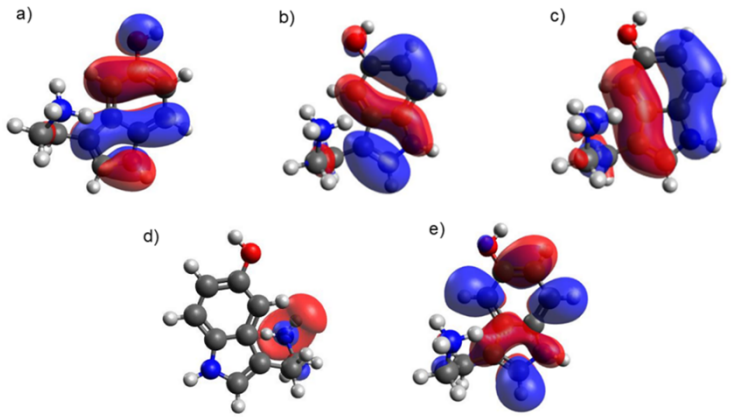

Fig. S8. MOs of isolated SERO involved in the lower energy electronic excitations: a) HOMO, b) HOMO-1, c) HOMO-2, d) LUMO, e) LUMO+1. Color codes: blue=N; gray=C; red=O, white=H.

The molecular orbitals (MOs) involved in the lower energy excitations of SERO, and the calculated excitation spectrum are shown in Fig. S8 and S9, respectively. As can be seen, SERO absorbs in the UV region. The lowest energy bands, peaked at 267 nm and 245 nm, are composed essentially by two excitations (see Fig. S9). The main components of these bands correspond to the HOMO→LUMO+1 and to the HOMO-1→ LUMO+1 transitions, respectively. Higher energy peaks (*e.g.,* at 222 nm, 207 nm, and 198 nm, associated to HOMO→LUMO+2, HOMO-2→LUMO+1, and HOMO→LUMO+5 excitations, respectively) should not play a relevant role in the electronic excitation behaviour of the MDAP+SERO complex.

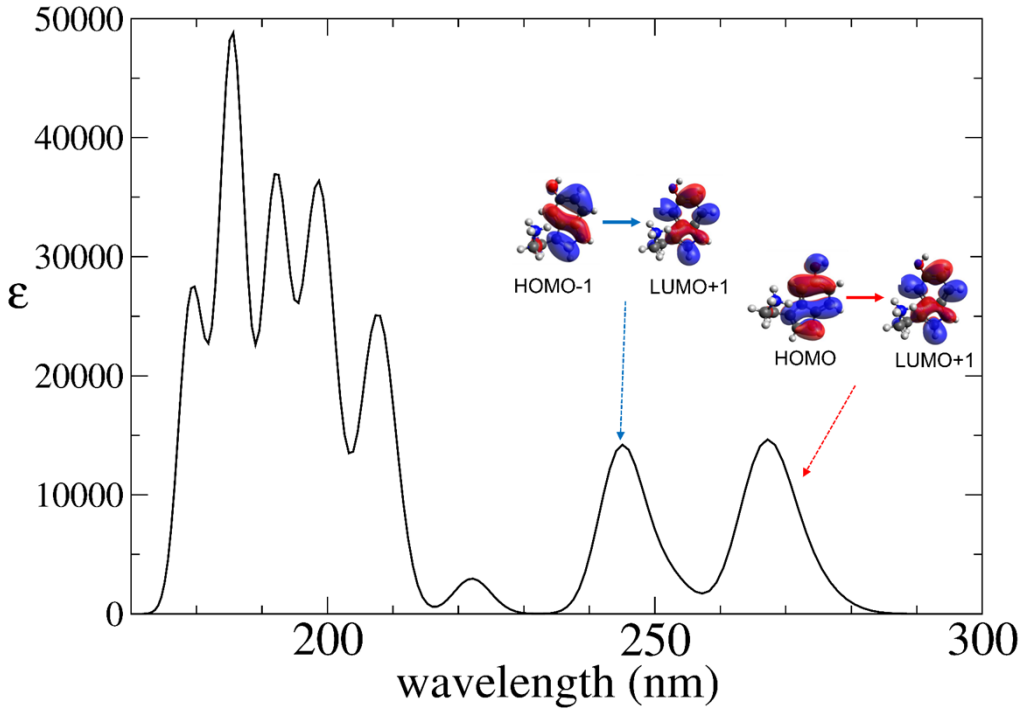

Fig. S9. Simulated UV-vis spectrum for isolated SERO in vacuum. The wavelength (λ, nm) and oscillator strength (f) of the components of the two highest-wavelength bands are also reported. The MOs involved in the main components of the two highest-wavelength bands are shown in the insets.

S3.2 MDAP

MDAP has been used as reporter dye in the nanozeolite receptors described in Ref.[4] It is characterized by four condensed aromatic units and a planar geometry.

The MOs involved in the lower energy electronic excitations are, as expected, mainly localized on the aromatic part of the molecule (see Fig. S10). The simulated spectrum is shown in Fig. S11, along with the bands' assignment. In particular, the highest-wavelength peak (356 nm) is ascribable to the HOMO→LUMO excitation, while the peak at 305 nm is due to the HOMO→LUMO+1 excitation. At lower wavelengths, the band peaked at 223 nm involves HOMO-2→LUMO and HOMO-2→LUMO+1 excitations, while the band at 188 nm is due to the HOMO-1→LUMO+2 transition.

As expected, the computed wavelength values are lower than those experimentally reported in Ref.[4], also because here we are considering an isolated MDAP in vacuum in its minimum energy structure (at 0 K), so thermal and solvent effects are not accounted for in the present calculations. Nonetheless, these calculations allow one to have a clear-cut assignment of the MDAP absorption bands in terms of electronic excitations, which will be of key relevance for the characterization of the electronic transitions of the MDAP+SERO complex.

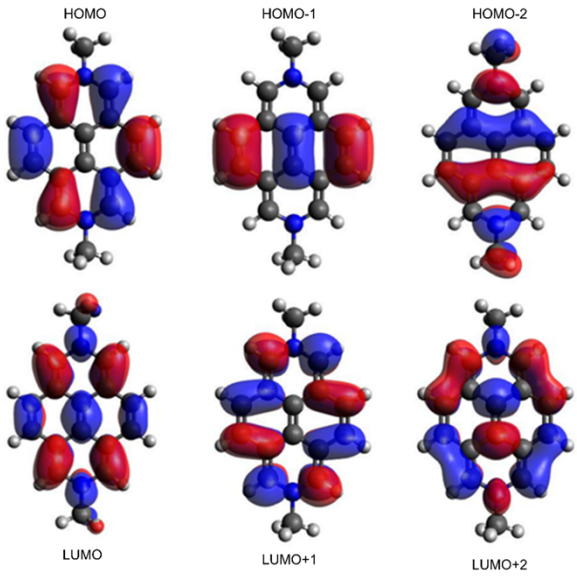

Fig. S10. Molecular orbitals of isolated MDAP involved in the electronic excitation spectrum shown in Fig.S11. Color codes: blue=N; gray=C; red=O, white=H.

The same approach – namely, TD-DFT/CAM-B3LYP/6-311++G(df,pd) – was adopted to compute the electronic excitations for the MDAP molecule extracted from the minimum energy structure of the (MDAP)ZL system. The MOs involved in the electronic excitations were analogous to those found for MDAP optimized in vacuum, as well as the band assignments.

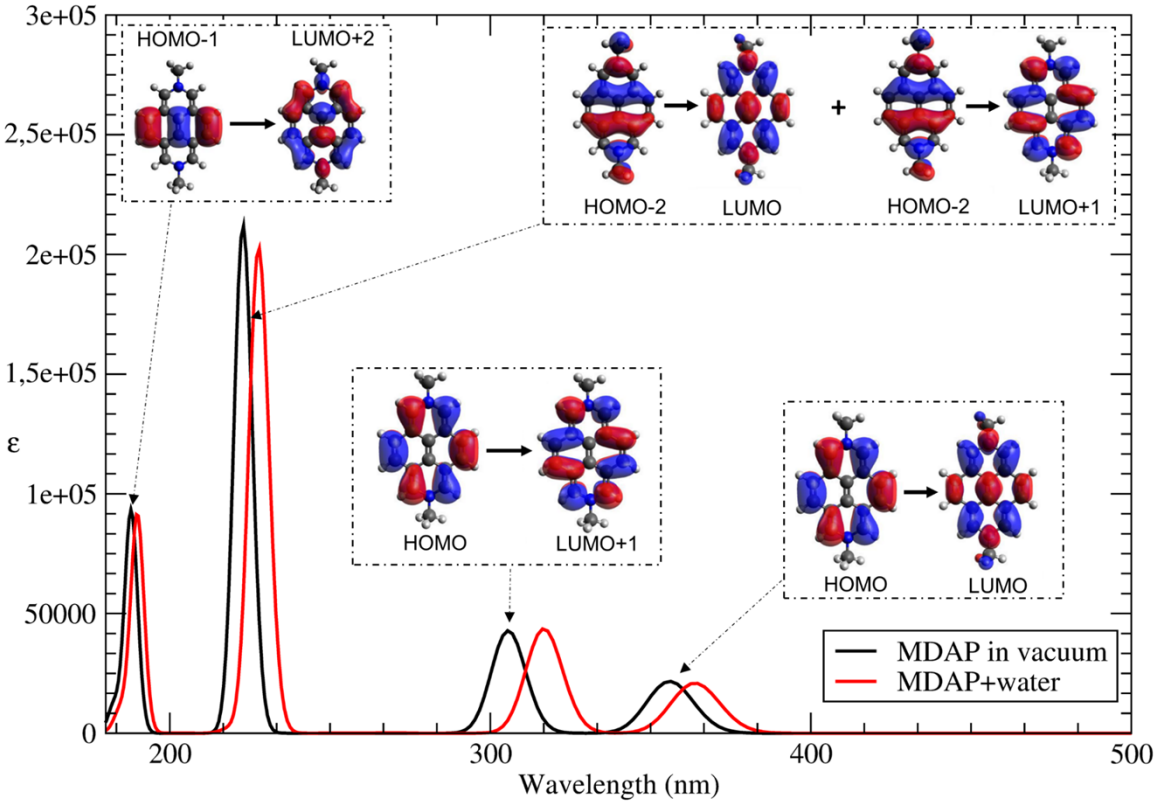

Fig. S11. Simulated UV-vis spectra for isolated MDAP in vacuum (black line) and for a cluster model of hydrated MDAP extracted from the minimum energy structure of the (MDAP)ZL system (red line). Band assignments in terms of electronic excitations is shown in the insets, along with the involved MDAP MOs.

However, the lower energy excitations were slightly red-shifted, *e.g.*, the HOMO→LUMO and HOMO→LUMO+1 transitions were found at 367 nm and 317 nm, respectively. Such modest red-shift of the lowest-energy excitations may be due to the geometry of MDAP extracted from optimized (MDAP)ZL, which is slightly distorted if compared to the optimized structure of MDAP in vacuum.

S4. Simulated UV-Vis spectra for (SERO)ZL, (MDAP)ZL and (MDAP+SERO)ZL minimum energy structures from cluster models

S4.1 Simulated UV-Vis spectra of MDAP and SERO from cluster models

As explained in Section S1.4, the UV-Vis spectra of the investigated host-guest systems were computed using cluster models constituted by the organic guest species and the surrounding water molecules, extracted from the pertaining minimum energy structures. To incorporate the effect of zeolitic water in the electronic spectra calculations, we choose an explicit description of water molecules. The simplest approximation is to treat the H and O atoms as charged points, hence, using a Molecular Mechanic (MM) model. One of the most used methods to obtain the partial charges in MM approaches with fixed charge force-fields is the Restrained ElectroStatic Potential (RESP).[27]

This method generates partial charges such as to reproduce the electrostatic potentials of molecules in the gas phase calculated at the HF/6–31G* level. In this work, the charges +0.34195 and -0.6839 were assigned to the water hydrogen and oxygen atoms, respectively.

Such an approach was tested on the minimum energy structure of (MDAP)ZL obtained from the periodic calculations. Specifically, in order to generate a cluster model for the calculation of the excited states of MDAP with a MM treatment of water molecules, the coordinates of the H_2Os surrounding MDAP (as well as those of MDAP) were extracted from the (MDAP)ZL minimum energy structure, to then carry out a TD-DFT calculation including the first twenty excited states. The model, shown in Fig. S12, comprises MDAP (QM treatment) and 43 H_2Os (MM treatment). The electronic spectrum computed with this approach is shown in Fig. S11, along with the previously discussed spectrum of isolated MDAP in vacuum. The results of the TD-DFT calculations indicated that the band assignment and the shape of the molecular orbitals involved in the excitations are the same as for isolated MDAP. The comparison of the two spectra in Fig. S11 indicates that all bands obtained for hydrated MDAP are red-shifted with respect to isolated MDAP. However, both the HOMO→LUMO and HOMO→LUMO+1 excitations (364 nm and 316 nm, respectively) were slightly blue-shifted with respect to the values obtained for the same MDAP geometry, but in the absence of water molecules (367 nm and 317 nm).

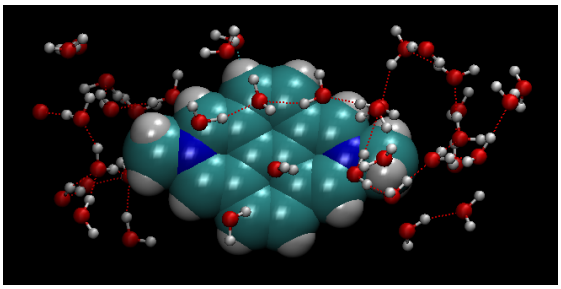

Fig. S12. The cluster model extracted from the minimum energy structure of (MDAP)ZL, consisting of MDAP+43 H_2O molecules. MDAP (large spheres) is treated at the TD-DFT/CAM-B3LYP/6-311++G(df,pd) level (QM) while H_2O molecules (ball-and-stick) are treated as point charges (MM).

In the spectrum of hydrated MDAP (Fig. S11), the band at 227 nm involve HOMO-2→LUMO and HOMO-2→LUMO+1 excitations, while the band at 190 nm is due to the HOMO-1→LUMO+2 transition. Nonetheless, these higher-energy transitions of MDAP should not play a relevant role in the sensing mechanism, as suggested by the experimental UV-vis spectra reported in Ref.[4].

To validate the point-charge treatment of the water molecules, we considered an upgraded model, in which some water molecules were treated at the TD-DFT/CAM-B3LYP/6-311++G(df,pd) level, like MDAP. To limit the computational cost, such approach was applied only to the eight water molecules closest to MDAP, i.e. those that should likely have a stronger interaction with the dye. The remaining

H_2Os were treated as RESP point charges like in the previous model. On this system, a TD-DFT calculation comprising the first twenty excited states was performed. The HOMO→LUMO and HOMO→LUMO+1 excitations were found at 368 nm and 320 nm, respectively, i.e. slightly red-shifted with respect to the values calculated using a point-charge treatment for all water molecules. Such a small difference justifies therefore the use of a RESP model for the description of surrounding H_2O molecules in the calculations of MDAP electronic excitations. Hence, a RESP model for water was adopted for the calculation of the electronic excitation in the case of hydrated SERO as well.

The first twenty excited states of SERO were calculated using the TD-DFT method (CAM-B3LYP/6-311++G(df,pd)), on a cluster model (Fig. S13a) cut from the periodic minimum energy structure of (SERO)ZL. The cluster model comprises SERO and the 46 surrounding H_2Os, the latter treated with the RESP model. The electronic spectrum computed for this model has been compared with that of isolated SERO (Fig. S13b). As can be seen, the addition of the solvent causes a modest red-shift of the highest wavelength peak (from 267 nm to 272 nm).

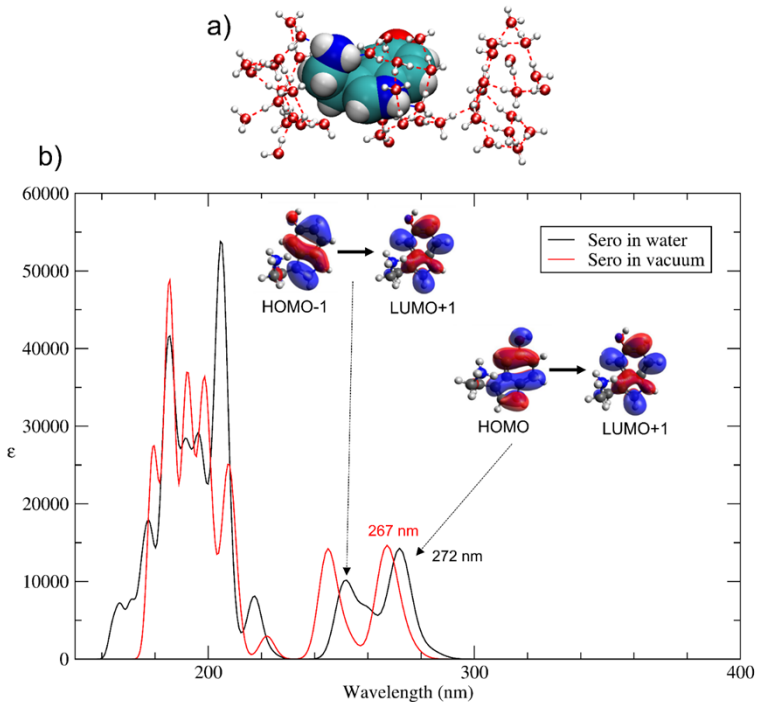

Fig. S13 a): Cluster model extracted from the minimum energy structure of (SERO)ZL, consisting of SERO+46 H_2O molecules; b): simulated UV-vis spectrum for the cluster model. The spectrum of isolated SERO in vacuum is also reported for comparison.

S4.2 Simulated UV-Vis spectrum of MDAP+SERO complex from cluster model

According to Grimm et al,[4] by titrating the (MDAP)ZL nanozeolite receptor with SERO, a strong quenching of the MDAP emission was observed. Such a change was accompanied by the appearance of a new band (430-550 nm) in the UV-vis spectra. The formation of the MDAP+SERO complex in

ZL, stabilized by zeolitic water, may therefore rationalize from a microscopic viewpoint the experimental observations on the SERO detection with the nanozeolite receptors (MDAP)ZL.[4] To substantiate this point, we simulated the UV-vis spectrum of the MDAP+SERO complex using a cluster model extracted from the (MDAP+SERO)ZL minimum energy structure.

The electronic excitation calculations on hydrated MDAP and SERO – whose coordinates were taken from the minimum energy structures of systems (MDAP)ZL and (SERO)ZL, respectively – have shown that a QM treatment of the organic moiety at the TD-DFT/CAM-B3LYP/6-311++G(df,pd) level combined to a MM description of water with a RESP point charge model represents a convenient accuracy vs. computational cost compromise. Therefore, this QM/MM approach has been employed to calculate the electronic excitations of the MDAP+SERO complex as well. The coordinates of the MDAP+SERO complex and the surrounding H_2Os were extracted from the (MDAP+SERO)ZL minimum energy structure. The cluster model (Fig. S14) comprises MDAP+SERO (QM treatment) and 37 H_2Os (MM treatment), and was subjected to a TD-DFT calculation of the first 50 excited states. A comparison of the simulated UV-Vis spectra of the hydrated MDAP+SERO complex with those obtained for the hydrated MDAP and SERO components is shown in Fig. S15.

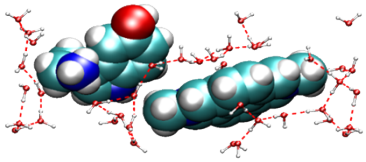

Fig. S14. Cluster model extracted from the minimum energy structure of (MDAP+SERO)ZL used to calculate the electronic excitations of the MDAP+SERO intermolecular complex.

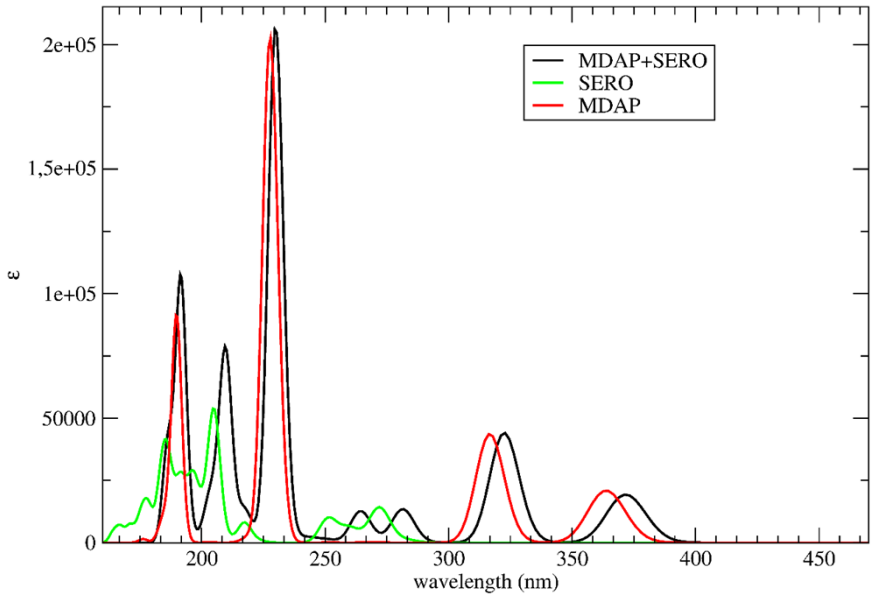

Fig. S15. Comparison of the UV-Vis spectra calculated from cluster models extracted from the minimum energy structures of the (MDAP+SERO)ZL, (MDAP)ZL, and (SERO)ZL periodic models.

The spectrum of the MDAP+SERO complex show similarities with the spectra calculated for the individual MDAP and SERO units. However, there are some important differences. First of all, the peaks corresponding to the HOMO→LUMO and HOMO→LUMO+1 transitions of isolated MDAP are displaced toward longer wavelengths. Indeed, in the MDAP+SERO intermolecular complex, these bands undergo significant red-shifts - from 364 nm to 372 nm, and from 316 nm to 322 nm, respectively. Additionally, the two MDAP bands at higher energy are red-shifted as well – namely, from 227 to 230 nm, and from 190 to 192 nm – in passing from MDAP to the MDAP+SERO complex. On the other hand, in the MDAP+SERO complex, the bands localized on SERO are blue-shifted with respect to the values found for SERO alone, in particular those pertaining to the two lower energy excitations of SERO (240-280 nm region). These observations are confirmed by a detailed band assignment (Table S2), along with the identification of the MOs involved in the electronic excitations (Fig. S16). It is worth noting that, although few MOs are spread on both moieties (i.e., MOs 117, 118 and 135 in Fig. S16), most of the MOs are localized on either MDAP or SERO only.

Remarkably, the data in Table S2 reveal that, in the spectrum of the complex, two very low-intensity bands are found at 457 nm and 414 nm - *i.e.*, at wavelengths much higher than those associated to the MDAP and SERO units (see also Fig. S17, inset).

Excitation	λ	f
108→109 HOMO→LUMO	**456.77**	**0.0001**
107→109 HOMO-1→LUMO	**414.31**	**0.0002**
108→110 HOMO→LUMO+1	403.13	0.0000
106→109 HOMO-2→LUMO	371.74	0.1181
107→110 HOMO-1→LUMO+1	**369.53**	**0.0014**
106→110 HOMO-2→LUMO+1	322.51	0.2724
108→115 HOMO→LUMO+6	281.48	0.0828
107→115 HOMO-1→LUMO+6	264.79	0.0534
108 →116 HOMO→LUMO+7	263.23	0.0248
102→109 HOMO-6→LUMO	229.82	1.1337
106→112 HOMO-2→ LUMO+3	217.01	0.0668
107→116 HOMO-1→ LUMO+7 **108→124 HOMO→ LUMO+15**	210.39	0.1345
107→117 **HOMO-1**→ LUMO+8 **108→124 HOMO→ LUMO+15**	209.59	0.3042
107→118 **HOMO-1**→ LUMO+9	204.50	0.0513
108→123 HOMO→ LUMO+14	202.74	0.0508
100→110 HOMO-8→LUMO+1	202.50	0.0147
103→111 HOMO-5→LUMO+2	191.57	0.5321
108→135 HOMO→ LUMO+26	186.76	0.1563

Table S2. Band assignment for the simulated UV-Vis spectrum of the hydrated MDAP+SERO complex (shown in Figs. S15 and S17) in terms of MOs (see Fig. S16). The green and red colors refer to MOs mostly localized on MDAP and SERO, respectively, while black refers to MOs localized on both moieties. Excitations colored in red and green can be considered as belonging to MDAP and SERO, respectively, as individual units, while black refers to charge-transfer transitions. For the higher-energy bands, only the main component(s) of the transitions have been included in Table S2.

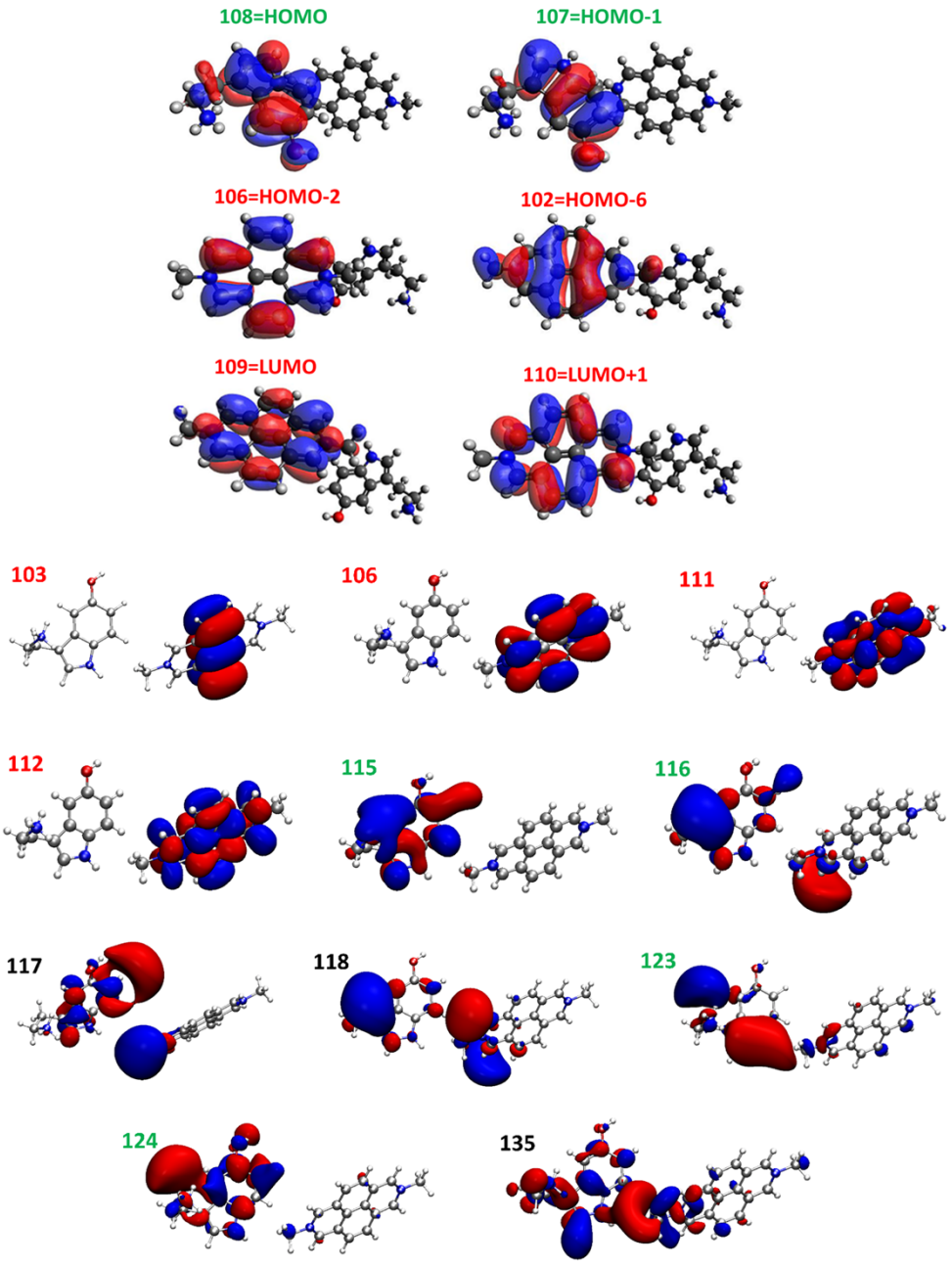

Fig. S16. Molecular orbitals of the MDAP+SERO complex involved in the electronic excitations reported in Table S2. MOs localized on MDAP and on SERO are labeled in red and green, respectively. MOs localized on both MDAP and SERO moietes are labeled in black.

Such new bands are associated to the HOMO→LUMO and HOMO-1→LUMO excitations in the MDAP+SERO complex, respectively. Importantly, while the HOMO and HOMO-1 MOs of the complex are localized only on SERO, the LUMO is completely localized on MDAP (see Fig. S16). Hence, these excitations – absent in the individual spectra of MDAP and SERO in ZL – are indeed charge-transfer transitions from SERO to MDAP, where SERO acts as a donor and MDAP acts as an acceptor of electron density, as also proposed in Ref.[4].

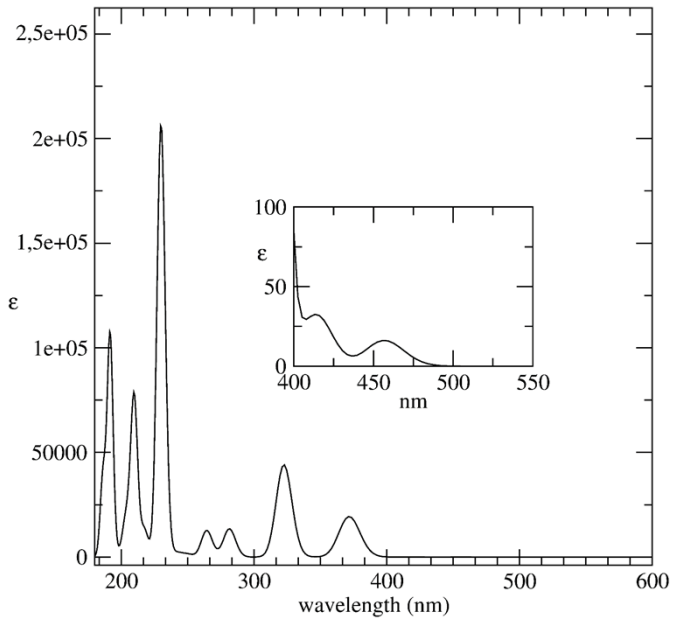

Fig. S17. Simulated UV-vis spectrum for the cluster model extracted from the (MDAP+SERO)ZL minimum energy structure. The low-intensity charge-transfer bands at 457 nm and 414 nm are shown in the inset.

By comparing these findings with those reported in Ref.[4], it emerges that, beside the agreeement on the emergence of charge-transfer bands upon formation of the MDAP+SERO complex, the present results underestimate both the wavelength and the intensity of the charge-transfer signal experimentally found – i.e. the growing of a broad band in the ≈430–550 nm range when the nanozeolite receptors (MDAP)ZL were titrated with serotonin. Actually, theoretical calculations presented in Ref.[4] predicted CT bands in such wavelength range as well. Such spectra were computed at the TD-DFT/PBE0/def2-TZVP level of theory on a system constituted only by the MDAP and SERO molecules. The coordinates of such molecules were extracted by a previously optimized cluster model constituted by two ZL unit cells, MDAP, SERO, and 24 surrounding H_2O molecules.[4] The effects of water on the electronic properties of the MDAP+SERO system were modeled by adopting an implicit solvent model for water in the TD-DFT calculations, namely the COSMO model.[30] Such literature results prompted us to use an implicit solvent model for water in the TD-DFT calculations of our MDAP+SERO complex, extracted from the optimized geometry of the periodic (MDAP+SERO)ZL system. Our aim was to analyze the effect of an implicit solvent description of water on the electronic excitations of the MDAP+SERO complex – especially on the CT ones, and to compare the outcomes with the previously discussed ones, obtained with a point-charge H_2O model. The results of this investigation are presented in the following paragraph.

S4.3. Effect of implicit solvent on MDAP+SERO UV-Vis spectrum

The model for testing the effects of implicit solvent was built by taking the coordinates of the MDAP+SERO complex from the (MDAP+SERO)ZL minimum energy structure (Fig. S6) without

solvating water molecules. Hence, such model comprises only MDAP and SERO, in the same geometry and orientation displayed in Fig. S14. On this cluster, first we performed as a reference a TD-DFT calculation without any solvent (i.e., in the vacuum); then, we repeated the calculation using the SCRF implicit solvent model for water.[31] Both calculations were performed at the TD-DFT/CAM-B3LYP/6-311++G(df,pd) level and by considering the first 30 excited states of the model.

A comparison of the computed electronic spectra of the MDAP+SERO complex in the vacuum, with implicit solvent, and with point-charge water is shown in Fig. S18.

It should be mentioned at the outset that the MOs involved in the MDAP+SERO excitations, both in the vacuum and with implicit solvent, are very similar to those obtained with the point charge H_2O model (see Fig. S16). The TD-DFT calculation in the vacuum – performed only as a reference – predicts CT excitations at considerably longer wavelenghts with respect to the point-charge model.

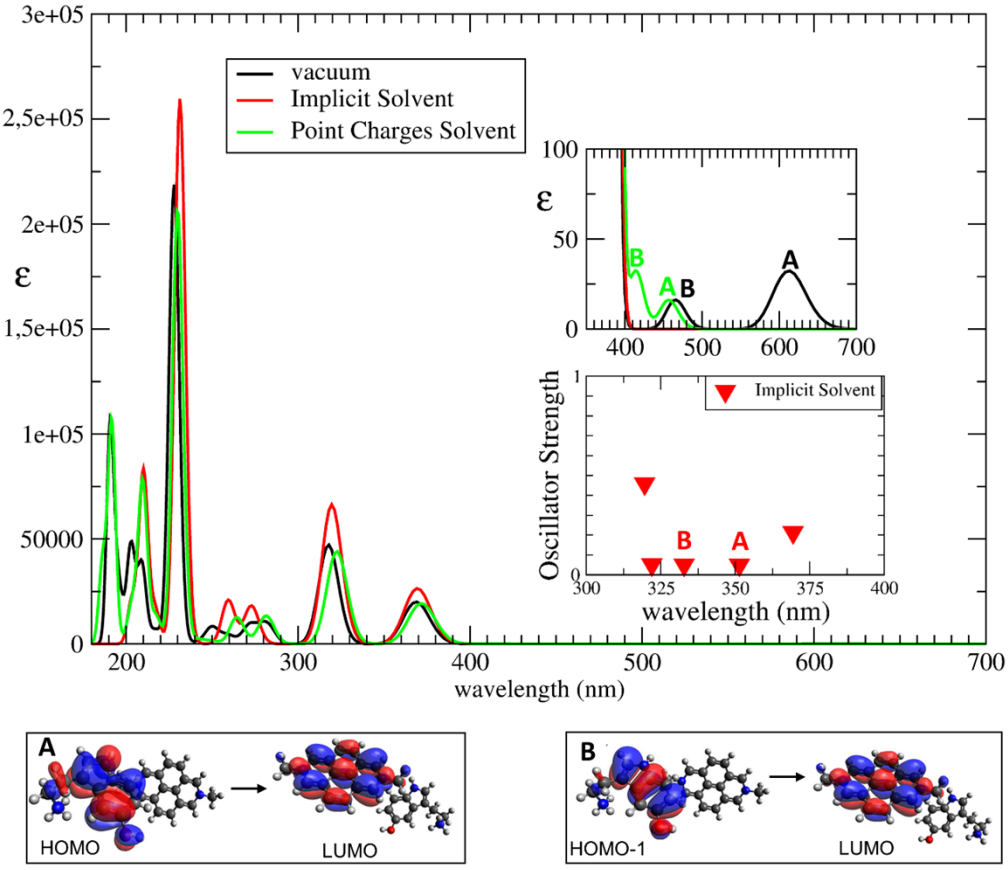

Fig. S18. Simulated UV-Vis spectra for the cluster cut from (MDAP+SERO)ZL minimum energy structure obtained in the vacuum (black), using an implicit solvent model (red), and using explicit solvent (green). The low-intensity bands associated to the HOMO→LUMO and HOMO-1→LUMO CT transitions (labeled as A and B, respectively) are shown in the insets.

Specifically, the HOMO→LUMO and HOMO-1→LUMO CT transitions – labeled as A and B in Fig. S18 - are found at 612 nm and 466 nm, respectively (Fig. S18, top inset). These values -especially

the former one – are clearly too high in comparison with the experiment, thus indicating that the MDAP+SERO complex in the vacuum is not a suitable model for the study of the electronic excitation behaviour of the MDAP+SERO complex in ZL, and that some description of the solvent (water) should necessarily be included in the model.

For example, the previously discussed point-charge H_2O model – adopted throughout this work– predicts the HOMO→LUMO CT band at 457 nm, *i.e.* within the experimentally found 430–550 nm range, although with a lower intensity.

By considering now the TD-DFT calculation with the implicit solvent model, the HOMO→LUMO and HOMO-1→LUMO CT excitations were found at 351 nm and 333 nm, respectively (Fig. S18, bottom inset) – i.e., at much lower values than the experimentally observed range. Such a result discourages the choice of an implicit solvent model for zeolitic water. Hence, implicit solvent water was no longer considered in all the models described in the following.

S4.4. Influence of Periodic Boundary Conditions on the choice of the cluster model

In performing calculations with periodic boundary conditions (PBC), there is not a clear-cut definition of the coordinates' origin. This fact may cause some issues when extracting a portion (a cluster) from a periodic structure. Indeed, in our case, an infinite sequence of SERO-MDAP pairs along the *c* direction is associated to the PBC. A truncated series of pairs is shown in Fig. S19, where the sequence MDAP-SERO-MDAP-SERO is depicted for the minimum energy structure of (MDAP+SERO)ZL.

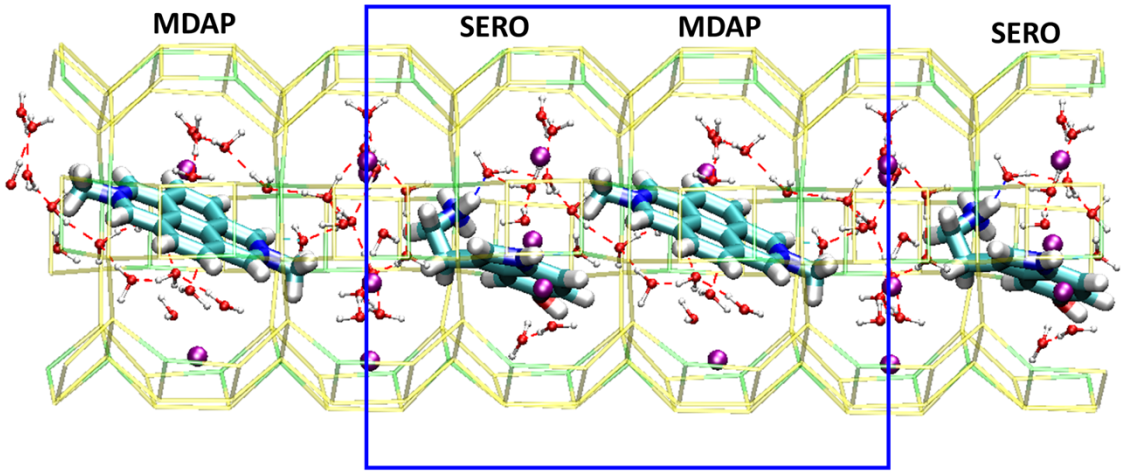

Fig. S19. Sequence of MDAP and SERO units encapsulated in ZL, representing the periodic images of the neighboring PBC structures along the ZL channel (*c* direction). Color codes as in Fig. S5. The blue lines indicate the PBC simulation cell along the *c* axis.

For the calculations reported until now, we have chosen the SERO-MDAP sequence because of the low value of the shortest intermolecular separation (3.2 Å). However, a second choice is possible –

namely, the MDAP-SERO 'inverted' cluster sequence, characterized by a higher value of the shortest intermolecular separation (5.6 Å) than the previous cluster, as illustrated in Fig. S20. On such an inverted MDAP-SERO pair, we performed a TD-DFT calculation in order to compare the electronic excitation properties of such alternative sequence choice with those obtained using the previously defined intermolecular complex, which is more 'compact'. The inverted complex was treated at the CAM-B3LYP/6-311++G(df,pd) level of theory and was "solvated" by 45 MM H_2O molecules, as shown in Fig. S20a. For comparison, the structure of the solvated 'compact' intermolecular complex is shown in Fig. S20b. The UV-Vis spectra calculated for the two models are compared in Fig. S21.

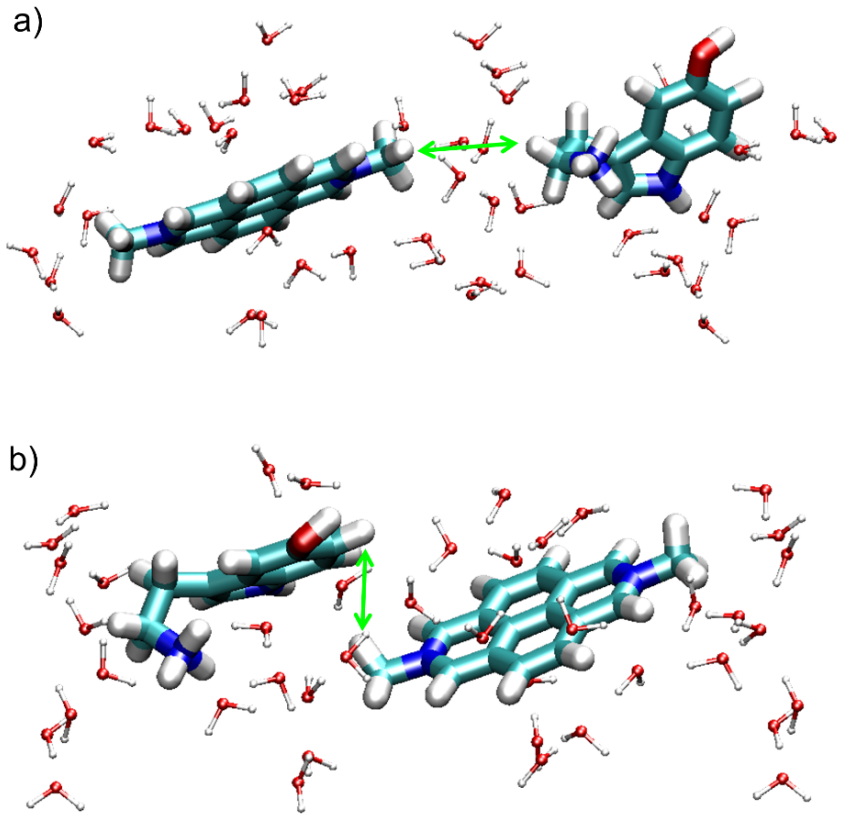

Fig. S20. Graphical representation of: **a)** inverted complex; **b)** 'compact' complex. The green arrows indicate the shortest intermolecular separation, namely 5.6 Å in **a)** and 3.2 Å in **b)**. Both geometries are estracted from the minimum energy structure of the periodic (MDAP+SERO)ZL system. Color codes as in Fig. S3.

In the spectrum of the inverted complex, the CT signals, predicted at 457 nm and 414 nm for the 'compact' complex, are missing. Indeed, the two highest-wavelength excitations, found at 368 nm and 330 nm in the spectrum of the inverted cluster, are fully localized on MDAP, and are associated to the HOMO→LUMO and HOMO→LUMO+1 excitations of isolated MDAP, respectively (see also Fig. S11). The absence of CT bands in the spectrum of the inverted complex could be rationalized by considering the large distance between the π-structures of SERO and MDAP in such an arrangement. Importantly, the above reported data justify the choice of the simulation cell size:

indeed, only one of the two closest SERO images can affect the optical properties of a given MDAP unit. On these bases, in the following calculations, only the MDAP+SERO 'compact' complex, characterized by the shortest intermolecular separation (3.20 Å), will be considered.

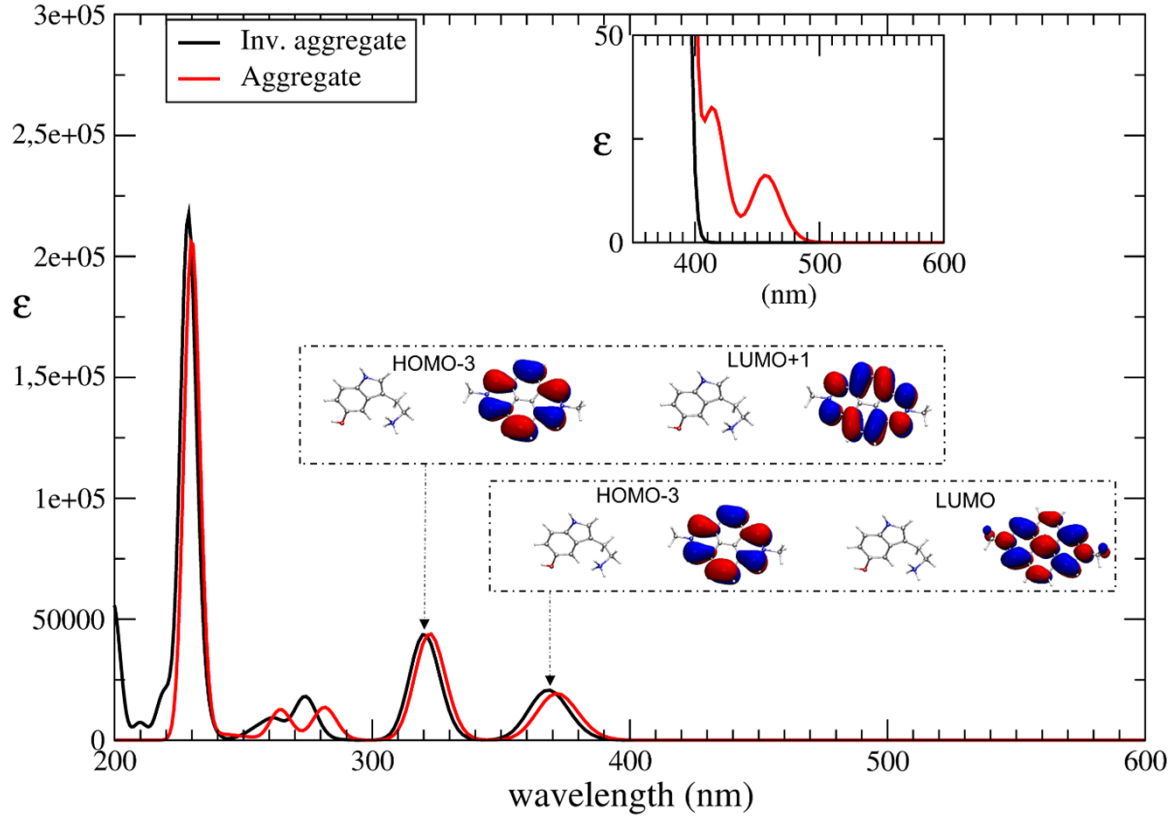

Fig. S21. Comparison of the UV-vis spectra calculated for the MDAP+SERO 'compact' complex and for the inverted complex. The top inset shows an enlargement of the 350-600 nm region, where only the CT bands of the 'compact' complex are present (at 457 nm and 414 nm). The bottom insets show the MOs involved in the lowest-energy electronic excitations of the inverted complex, fully localized on the MDAP unit.

S5. Structural information from AIMD simulations of (MDAP+SERO)ZL, (MDAP)ZL, and (SERO)ZL systems.

Until now, we have considered only 0 K structures, namely those deriving from geometry optimizations. On the other hand, the thermal motion, causing structural distorsions as well as rotational and/or traslational motion, may affect the system equilibrium properties in general. To evaluate these effects, we analyzed the room-temperature dynamics of the investigated systems by calculating radial distribution functions (g(r)s), thus providing an average structural picture of the three host-guest materials. Moreover, thermally-averaged electronic excitation spectra of the (MDAP)ZL and of the (MDAP+SERO)ZL systems were calculated on configurations sampled from the respective AIMD simulations.

All the three host-guest systems considered herein are stable along their room-temperature trajectories. MDAP remains located approximately in the center of the 12MR channel, as in the (MDAP)ZL minimum energy structure. Due to thermal motion, the angle formed by its molecular axis with the ZL channel axis slightly oscillates around 30°. However, in the simulated elapsed time (~42 ps), the molecule does not translate along the channel, which also contains zeolitic H_2Os. Also SERO, during the AIMD simulation, maintains its positioning close to the channel walls. Both $–NH_3$ and –OH groups remain, on average, hydrogen bonded to the framework oxygen atoms; moreover, the $–NH_3$ group forms hydrogen bonds with water molecules as well. With respect to their minimum energy structures, both MDAP and SERO show distortions from planarity of their π-conjugated systems. Such distorsions from planarity are also observed by considering the thermal behaviour of the complex (visually sketched in the "MDAP_SERO_ZL.mpeg" movie). As can be seen, the complex is stable at room temperature conditions. Specifically, the two units remain, on average, rather close to each other, even though a certain range of MDAP-SERO intermolecular separations is sampled along the simulations. The behaviour of the two component units in the complex does not appear to be much different with respect to that found when only MDAP or only SERO were enclosed in the ZL channel. In particular, whereas MDAP stays close to the channel center, SERO is located close to the pore walls, and it is hydrogen bonded to both framework oxygens and water molecules. Importantly, as observed in the (MDAP+SERO)ZL minimum energy structure, there are a few H_2Os located between MDAP and SERO, in order to screen the positive charges of these two moieties.

A more thorough insight on the structure of the three host-guest systems at room temperature conditions can be obtained from the radial distribution functions computed from AIMD trajectories.

S5.1 Radial distribution functions from the AIMD simulations.

The H_2O-H_2O radial distribution functions (g(r)) are reported in Fig. S22. The intense and narrow peaks at about 1 Å in all the O-H g(r)'s indicate the intramolecular O-H bonds. The peaks at 1.8 Å are relative to intermolecular O-H contacts, indicating strong H_2O-H_2O hydrogen bonding for all three systems – namely, (MDAP+SERO)ZL, (MDAP)ZL, and (SERO)ZL. The presence of strong hydrogen bonding is also confirmed by O-O g(r)'s that show the main peak at about 2.8 Å for all the three systems. Further O-O peaks, at 4.5 Å, indicate a close-to-liquid-phase structure for water inside the ZL channels. Such a structure is more pronounced for the (SERO)ZL system, and less pronounced for the (SERO+MDAP)ZL case. The quasi-liquid-water structure is also evidenced by a third O-O peak at about 7 Å.

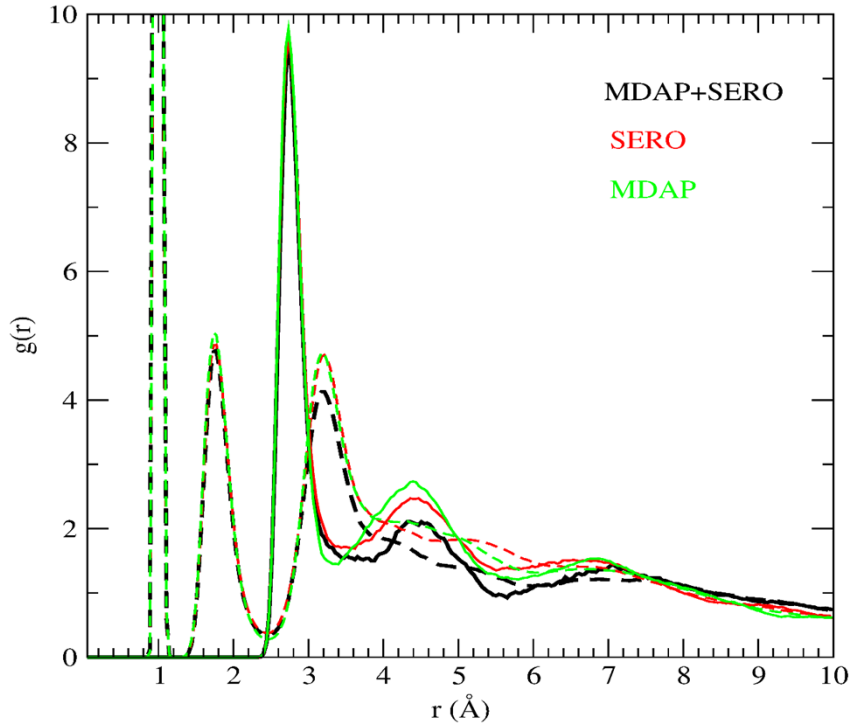

Fig. S22. H_2O radial distribution functions g(r)'s from the three room temperature AIMD simulations. Dashed lines represent O-H g(r)'s, while continuous lines are for O-O g(r)'s. Black lines refer to (MDAP+SERO)ZL, red lines to (SERO)ZL, green lines to (MDAP)ZL.

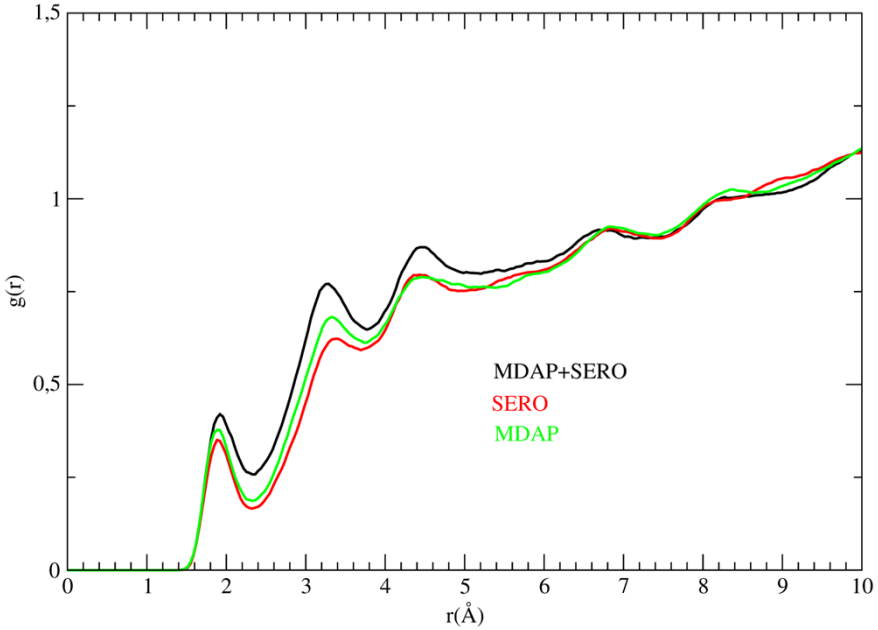

Fig. S23. The H_{water}-O_{frame} radial distribution functions g(r)'s calculated from the AIMD trajectories. The black line refers to (MDAP+SERO)ZL, the red line to (SERO)ZL, and the green line to (MDAP)ZL.

By inspecting Fig. S23, representing the g(r)'s for the H(water)-O(framework) contacts, it emerges that water is also interacting, via hydrogen bonding, with the framework oxygens, a typical behavior of zeolitic water. Such an interaction, detectable by the peaks at about 1.9 Å, is however weaker than the intermolecular H_2O-H_2O hydrogen bonding (at 1.8 Å) as reported in Fig. S22.

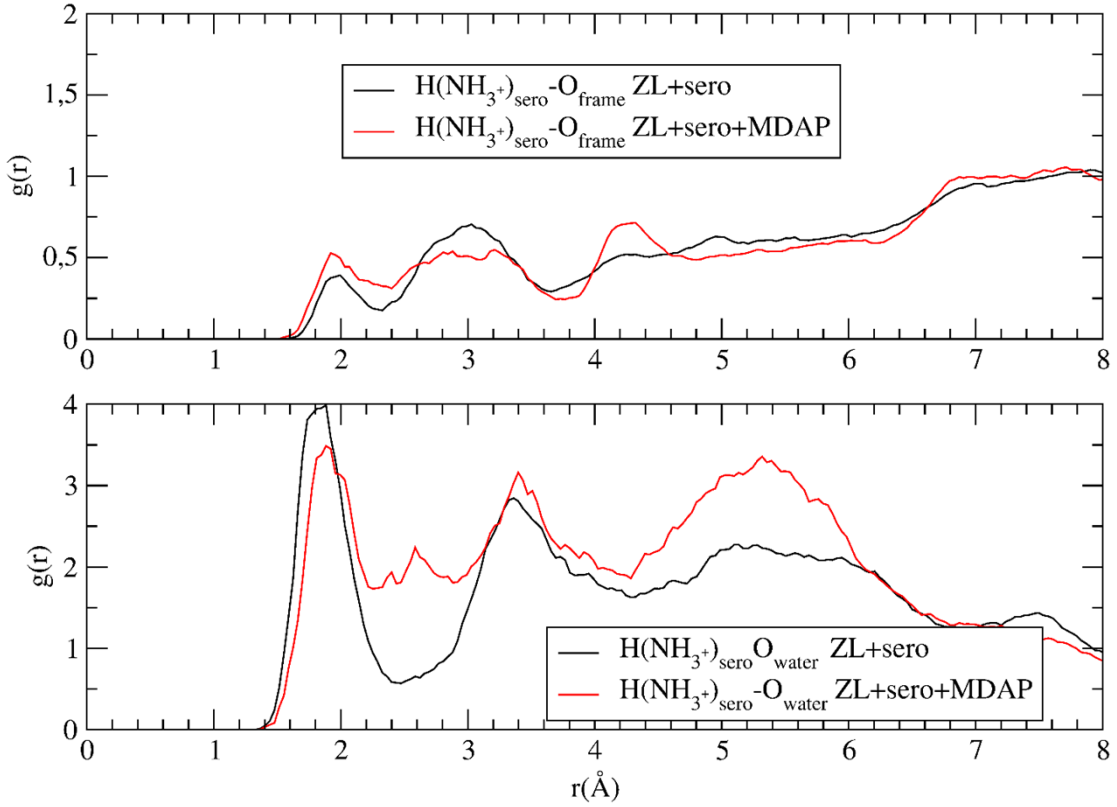

Fig. S24. Top panel: g(r) of the SERO $–NH_3^+$ protons with the ZL oxygens. Bottom panel: g(r) of the SERO $–NH_3^+$ protons with the water O atoms. Black lines refer to (SERO)ZL, red lines to (MDAP+SERO)ZL.

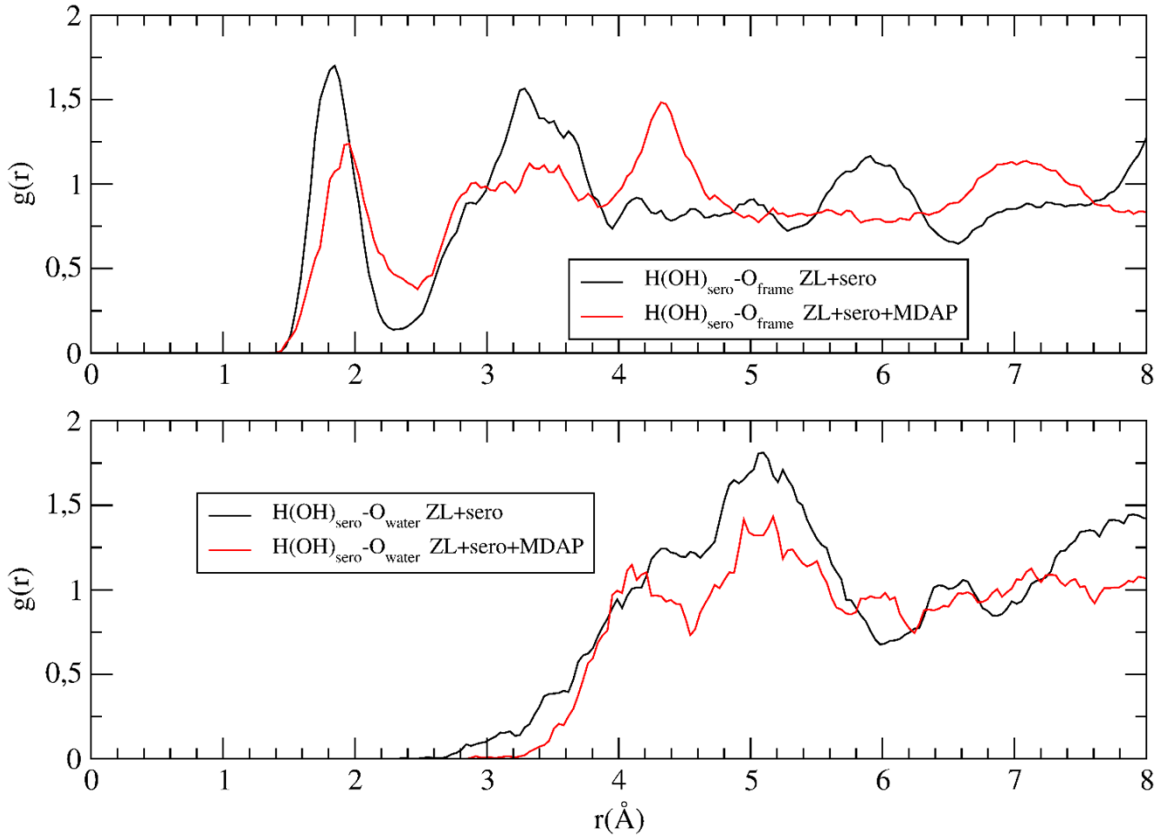

Fig. S25. Top panel: g(r) of the SERO -OH proton with the ZL framework oxygens in the (SERO)ZL and (MDAP+SERO)ZL systems. Bottom panel: g(r) of the SERO -OH proton with the water oxygens in the (SERO)ZL and (MDAP+SERO)ZL systems.

The SERO interactions with either water or ZL framework oxygens can be quantified by inspecting Figs. S24 and S25. The SERO ammonium protons strongly interact with water oxygens (1.9-2.0 Å), indicating hydrogen bonding. Such a hydrogen bonding is more pronounced in the (SERO)ZL system. The presence of MDAP in (MDAP+SERO)ZL system induces a weakening of such interaction. On the other hand, the interactions of the SERO ammonium protons with the framework oxygens, weaker than the interactions with water, are enhanced by the presence of the MDAP dication. This finding is in line with the experimental observations of Ref.[4] indicating a stronger affinity of SERO for the nanozeolite receptor (*i.e.*, the (MDAP)ZL system) compared to the parent ZL material. The SERO -OH group interacts quite strongly with the framework oxygens via its proton (as evidenced by the peak at 1.9 Å in Fig. S25, top). Such a strong hydrogen bonding interaction is only partially weakened (peak at 2.0 Å) by the presence of the MDAP species in the (MDAP+SERO)ZL system. The SERO -OH group practically does not interact with water, as can be seen from the bottom panel in Fig. S25.

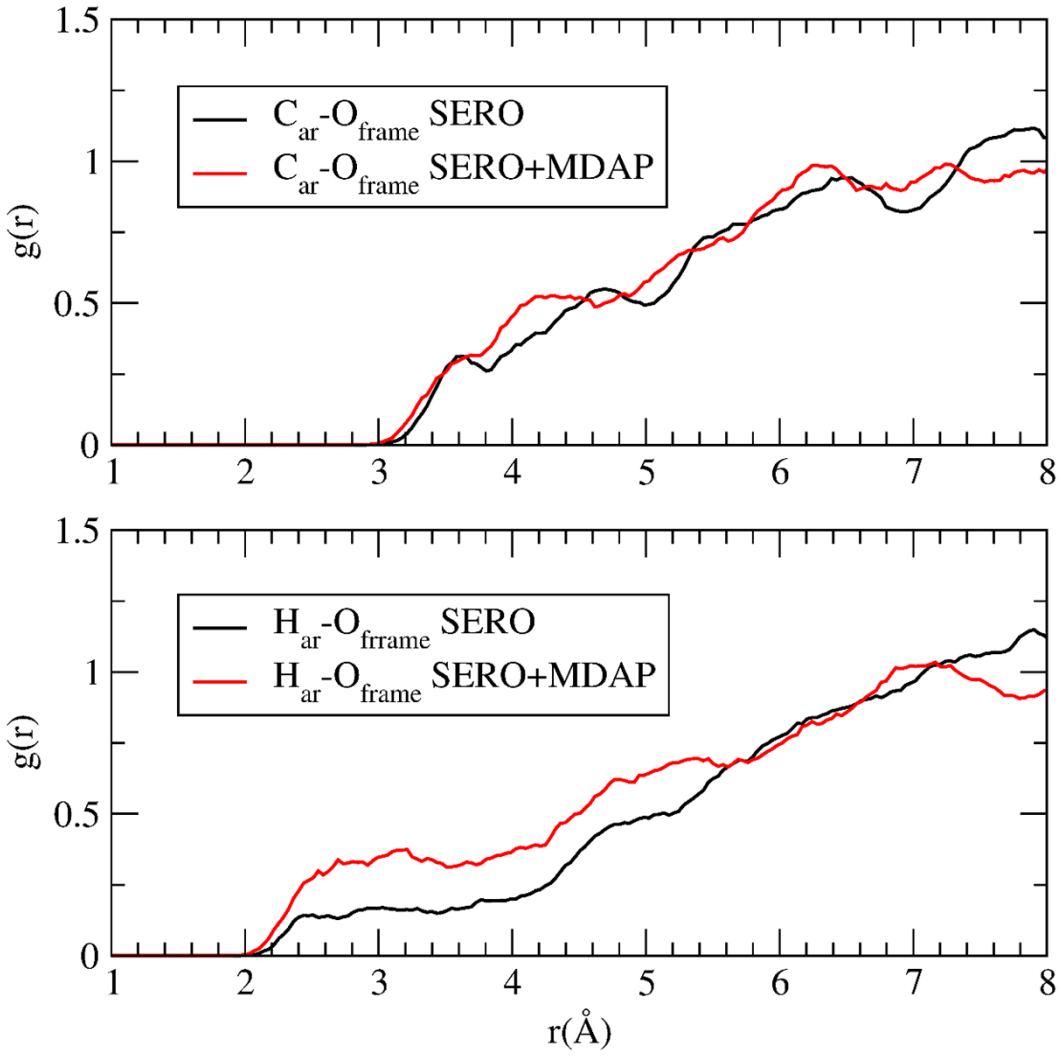

Fig. S26. Top panel: g(r) of the C atoms of the SERO aromatic part with the ZL framework oxygens in the (SERO)ZL and (MDAP+SERO)ZL systems. Bottom panel: g(r) of the H atoms of the SERO aromatic part with the ZL framework oxygens in the (SERO)ZL and (MDAP+SERO)ZL systems.

By considering the interaction of the aromatic part of SERO with ZL oxygens (Fig. S26), it emerges that the π-conjugated system of SERO further approaches the ZL walls in presence of MDAP. Overall, the analysis of the g(r)'s of SERO atoms with ZL and water oxygens suggests that the binding of SERO to the host is enhanced by the presence of MDAP, in line with experimental evidences.[4]

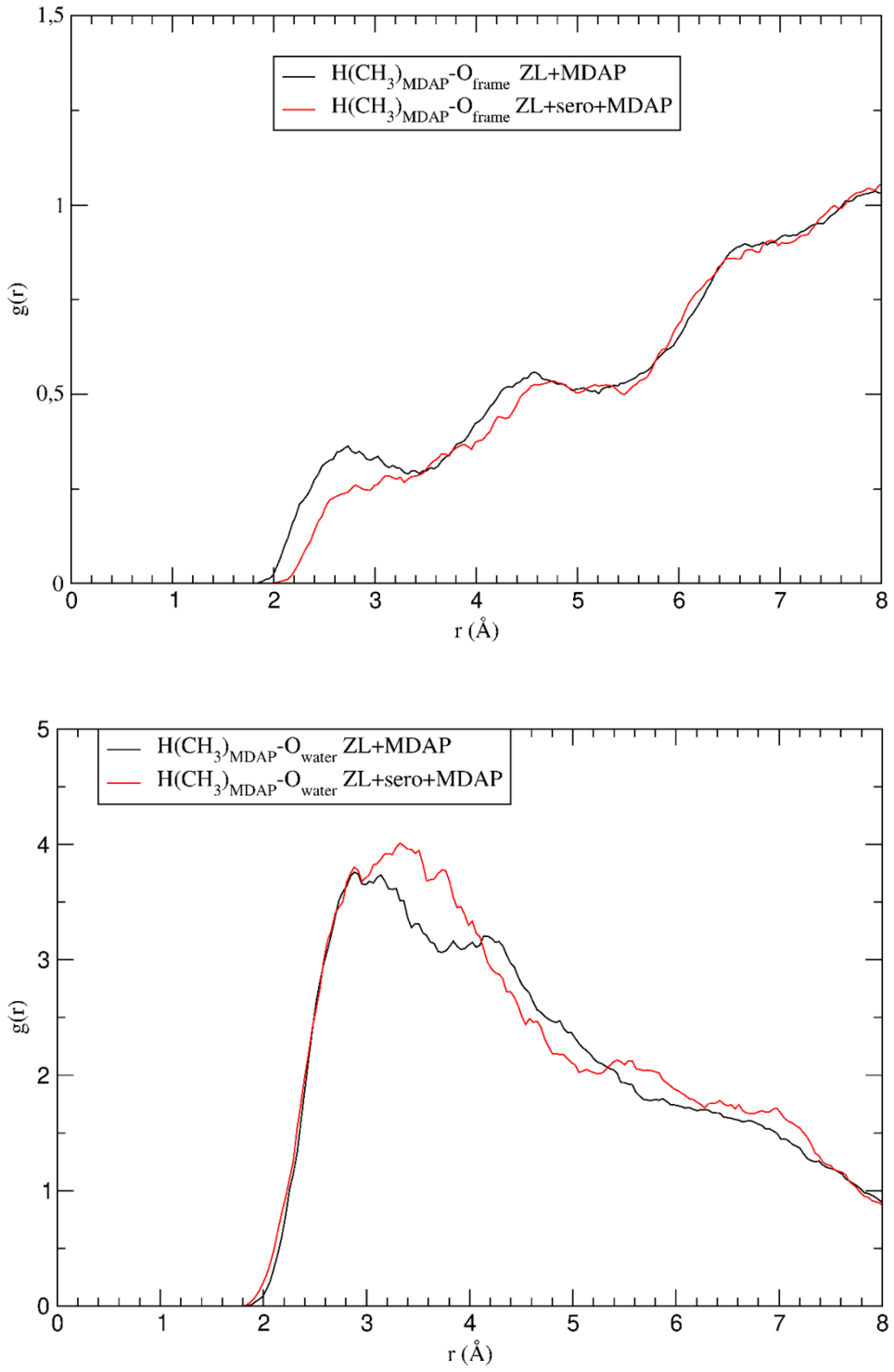

Fig. S27. Top panel: g(r) for the interaction of the $–CH_3$ protons of MDAP with the framework oxygens in the (MDAP+SERO)ZL and (MDAP)ZL systems. Bottom panel: g(r) for the interaction of the $–CH_3$ protons of MDAP with the water oxygens in the (MDAP+SERO)ZL and (MDAP)ZL systems.

The interaction of MDAP with its environment can be discussed by inspecting Fig. S27, showing the g(r)'s describing the contacts of the -CH_3 protons both with ZL framework and water oxygens. These g(r)'s are structured, but the broad peaks in the 2-3 Å range for the g(r) of such protons with the framework oxygens indicate weak interactions. Also, such interactions are furtherly weakened by the presence of the SERO species. Concerning the interactions of the MDAP -CH_3 protons with water oxygens (Fig. S27, bottom), relatively high peaks are present in the g(r)'s but at distances more akin to van der Waals interactions.

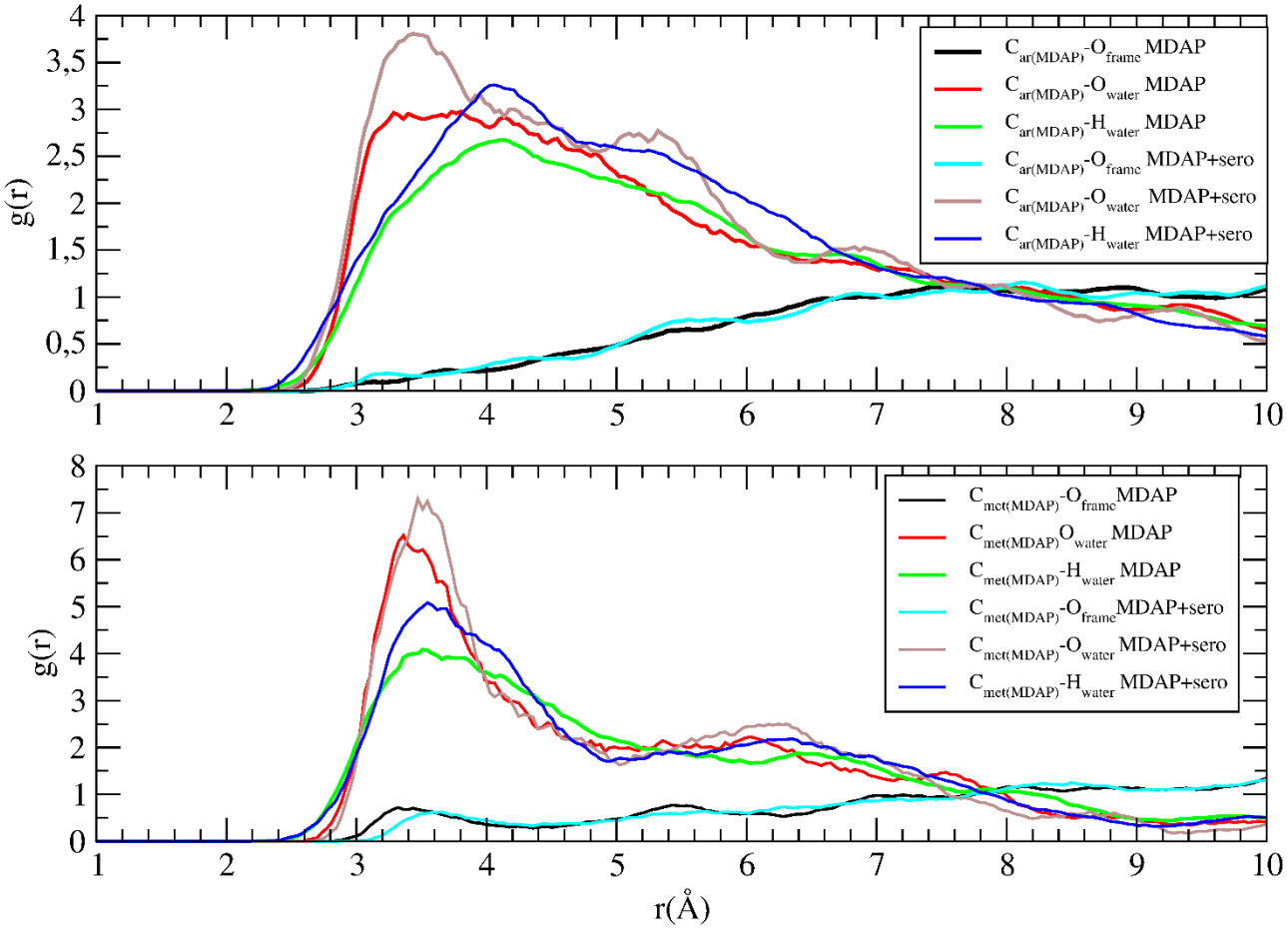

Fig. S28. Top panel: g(r) pertaining to the contacts of the aromatic MDAP C atoms with water and ZL oxygens in (MDAP)ZL and (MDAP+SERO)ZL systems. Bottom panel: g(r) pertaining to the contacts of the –CH_3 MDAP C atoms with water and framework oxygens in (MDAP)ZL and (MDAP+SERO)ZL systems.

By inspecting Fig. S28 it is possible to gather some interesting information on the behavior of MDAP when encapsulated in ZL. First, the bulk of the MDAP, represented by the group of aromatic carbon atoms, is quite far from the ZL walls, as its g(r) with the framework oxygens is practically unstructured. On the other hand, there are short-ranged interactions with the water oxygens (peak at 3.2-3.4 Å). Interestingly, such interaction of the aromatic C with water O becomes stronger in the presence of SERO. This fact suggests that, in the complex, water molecules are "screening" the Coulomb repulsive interactions between SERO and MDAP, both positively charged. This effect is

also evident in the g(r) of MDAP methyl C with the water oxygen atoms: the corresponding peak (Fig. S28, bottom panel) increases when SERO is present.

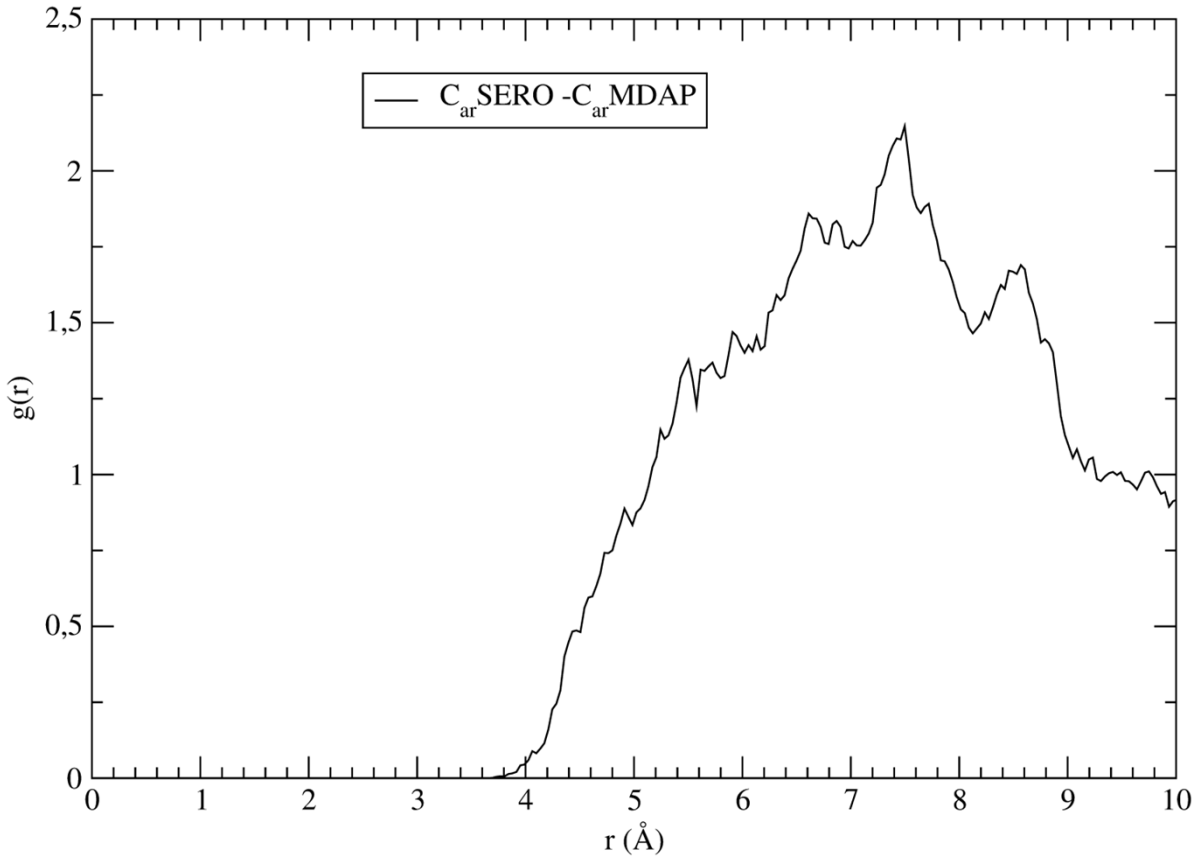

Fig. S29. Radial distribution function g(r) for the aromatic C atoms of SERO with the aromatic MDAP C atoms in the (MDAP+SERO)ZL system.

Relevant to the discussion on the behavior as sensor of the ZL when both SERO and MDAP are encapsulated, is the g(r) regarding the separation of the aromatic part of the two moieties. Actually, it is a charge transfer (CT) between a +1 species (SERO) to a +2 charged species (MDAP) that gives rise to a new band, thus allowing the (MDAP)ZL system to properly behave, upon SERO incorporation, as an extremely sensitive sensor for SERO. Such CT band is generated by an electron transfer from the π system of SERO to a π* state of MDAP. In Fig. S29, the g(r) pertaining to the separation of the two π systems indicates the distances manifold at which such CT event could occur.

S6. Thermally-averaged UV-Vis spectra calculated from cluster models

S6.1 MDAP

The thermally-averaged electronic spectrum was obtained by averaging the electronic excitations calculated for cluster models extracted from 15 configurations of the AIMD trajectory of (MDAP)ZL, and compared with the spectrum calculated for the minimum energy structure of MDAP in ZL using the same computational approach (see Fig. S30).

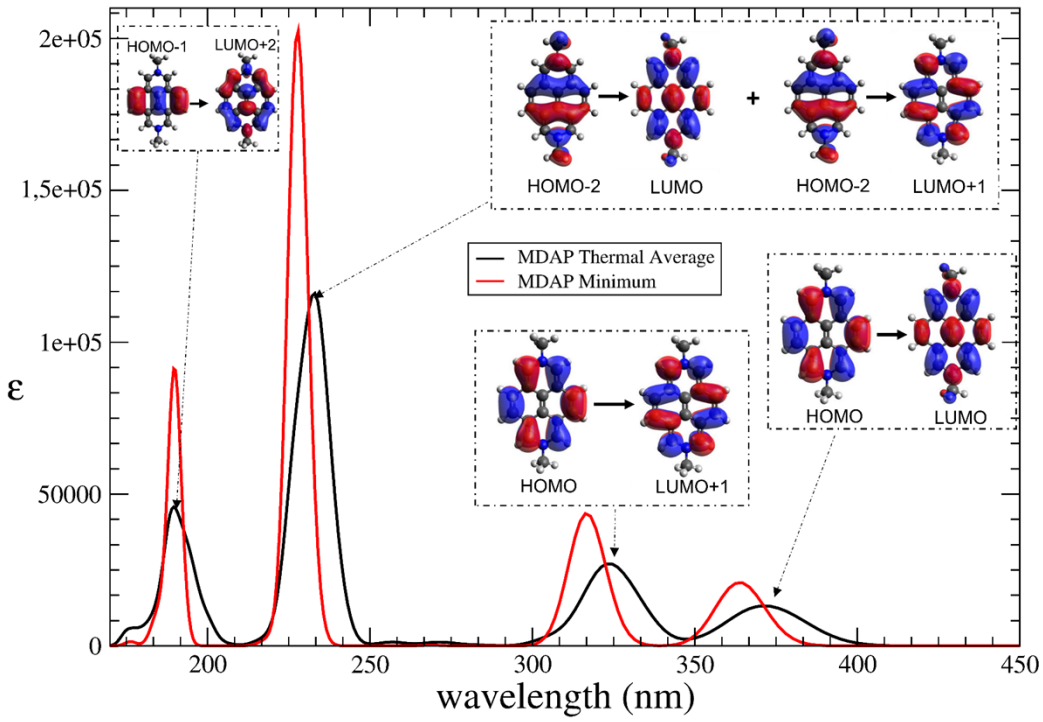

Fig S30. Comparison of UV-vis spectra obtained from thermal average of cluster models extracted from configurations sampled along the AIMD simulation of (MDAP)ZL (black line), and from the minimum energy structure of (MDAP)ZL (red line).

As can be seen in Fig. S30, the thermally averaged spectrum is more similar to the experimental spectrum[4] than the one obtained from the minimum structure, in terms of both relative intensity of the bands and wavelength values. Indeed, all bands of MDAP are broader and shifted towards longer wavelengths, in particular those related to the HOMO→LUMO and HOMO→LUMO+1 transitions. The cause of this red shift was sought by inspecting the MDAP geometry in the different configurations, evidencing that the red-shift is due to small distortions of the dye from planarity caused by its thermal motion in the ZL channel, as well as by the interactions of the dye with adjacent water molecules. These factors, especially the deviations from planarity of the MDAP aromatic system, are also at the origin of the appearance of very weak bands, in the 250-280 nm region.

S6.2 MDAP+SERO

The thermally averaged spectrum of the MDAP+SERO complex was computed as an average over cluster models cut from 25 configurations sampled from the (MDAP+SERO)ZL AIMD trajectory. In Fig. S31, it is compared with the spectrum calculated for the hydrated cluster model extracted from the (MDAP+SERO)ZL minimum structure. As observed for MDAP, in the thermally averaged spectrum of the MDAP+SERO complex the bands are broader and red-shifted with respect to the spectrum obtained from the minimum energy structure.

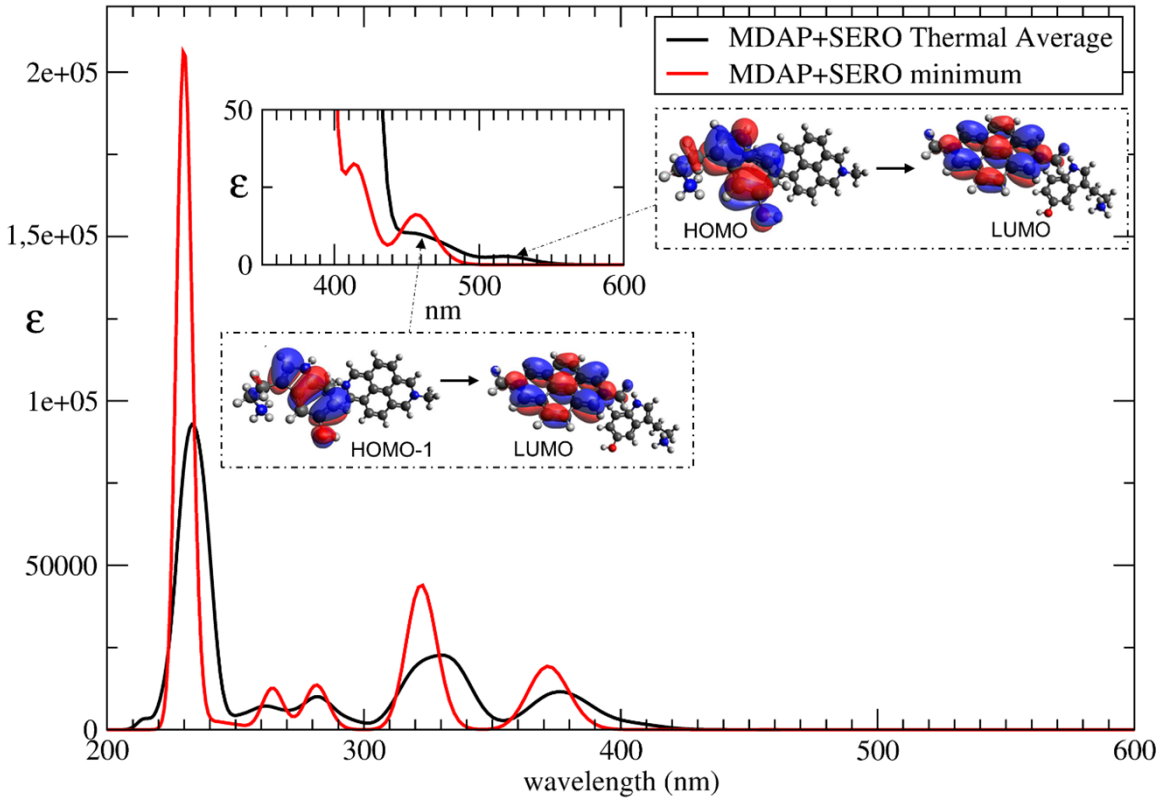

Fig S31. Comparison of the thermally averaged UV-vis spectrum obtained from cluster models extracted from configurations sampled along the AIMD simulation of (MDAP+SERO)ZL (black line), with the UV-Vis spectrum calculated from a cluster model extracted from the minimum energy structure of (MDAP+SERO)ZL (red line). The insets illustrate the CT bands, now appearing at 520 nm and at 460 nm, and the involved MOs.

Such a red-shift is particularly relevant for the CT bands, that now appear as a broad tail in the 450-550 nm region (see Fig. S31, inset) – hence, in agreement with the values experimentally found.[4] Specifically, two signals associated to the HOMO→LUMO and HOMO-1→ LUMO CT transitions can be distinguished in the 450-550 nm tail, at 520 nm and at 460 nm, respectively (see Fig. S31, inset). These CT excitations were found at 457 nm and 414 nm in the case of the corresponding minimum energy structure (see Fig. S17 and Table S2), indicating therefore that thermal effects play a key role in displacing the CT transitions towards longer wavelengths, i.e. in lowering the energy cost of electron transfer from SERO to MDAP. However, the CT band intensity, due to very small values of the oscillator strengths, remains very low.

Fig. S32 illustrates the comparison of the simulated UV-vis spectra of MDAP (red line) and MDAP+SERO (black line), both calculated as thermal averages from the AIMD simulations. Beside the appearance of the above-mentioned CT bands (which are obviously absent in the MDAP spectrum), the association of the neurotransmitter (SERO) with the reporter dye causes a reduction in the intensity of the MDAP peaks, in line with the experimental spectra trend.[4]

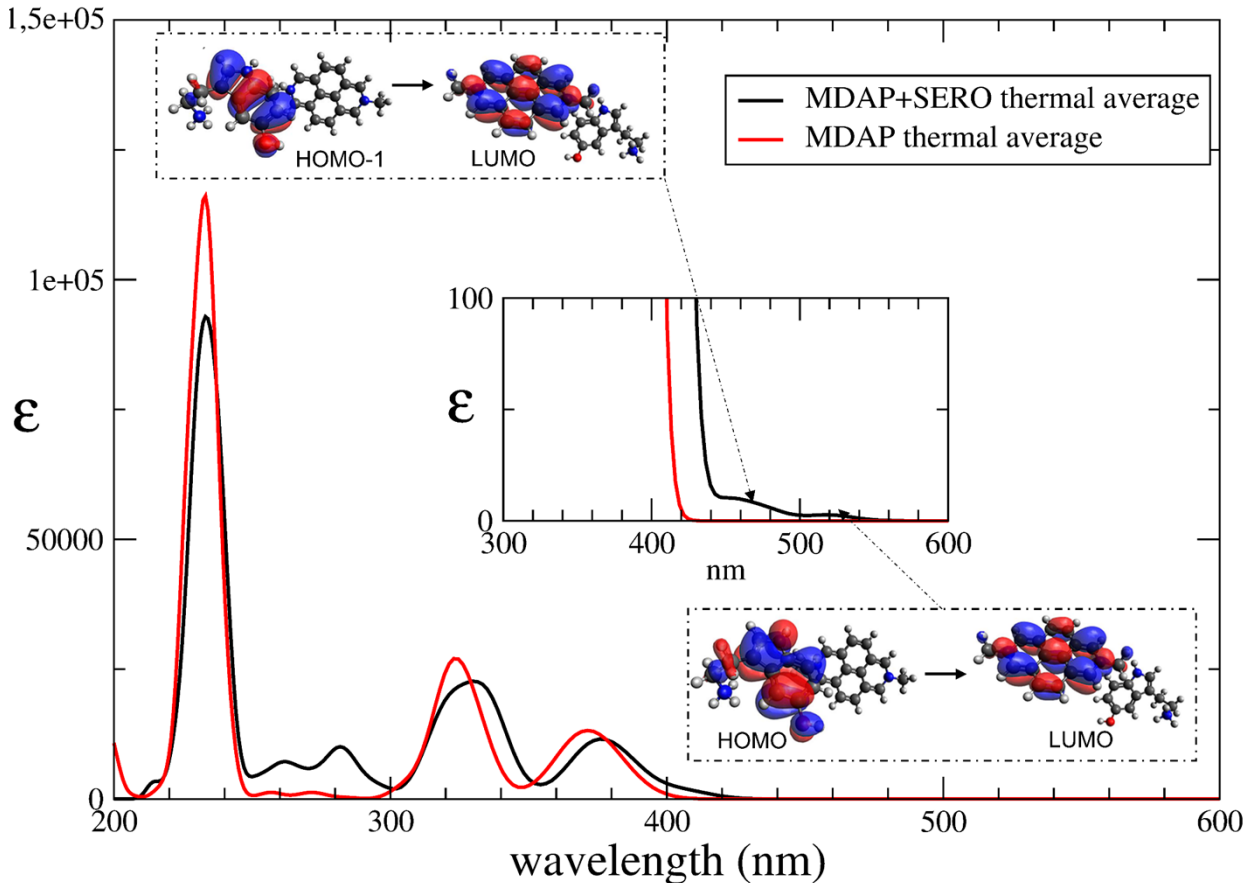

Fig. S32: Comparison of thermally averaged UV-vis spectra obtained from cluster models extracted from configurations sampled along the AIMD simulation of (MDAP+SERO)ZL (black line), and (MDAP)ZL (red line). The insets illustrate the CT bands at 520 nm and 460 nm, and the associated electronic excitations.

The molecular-level factors influencing the CT excitations (in particular, the wavelength and oscillator strength of the HOMO-LUMO transition) were assessed by analyzing a few geometrical parameters of the selected configurations. Specifically, we considered: i) the conformation of SERO; ii) the distortion from planarity of the aromatic structure of the two molecules; iii) the relative orientation of MDAP and SERO in the complex; iv) the MDAP-SERO separation, measured as the distance between the center of the SERO phenyl ring and the closest $–CH_3$ group of MDAP; v) the number and positioning of water molecules located between MDAP and SERO.

Concerning the wavelength of the HOMO→LUMO CT transition, regardless of the SERO conformation, configurations with π-systems in an "edge-to-face" type of arrangement and with a nearly planar geometry of both MDAP and SERO exhibit the HOMO→LUMO CT band at significantly longer wavelengths (above 500 nm) with respect to the minimum energy structure (457 nm). Conversely, configurations in which SERO and/or MDAP show considerable deviations from planarity are characterized by a HOMO→LUMO CT band at shorter wavelengths with respect to the minimum energy structure. Such energy increase of the HOMO→LUMO transition is likely due to

either HOMO stabilization (localized on SERO) or LUMO destabilization (localized on MDAP) as a consequence of the geometric distortion of the π-structure. Therefore, parameters ii) (deviations from planarity of the π-structure of MDAP and SERO) and iii) (reciprocal orientation of MDAP and SERO) appear to be the main factors influencing the CT band position, while their effect on the intensity is less pronounced. Nonetheless, the intensity of the CT band is slightly higher in configurations with a nearly edge-to-face MDAP-SERO orientation, and a π-structure geometry close to planarity.

Concerning the CT intensity, let us now examine parameters iv) and v). Indeed, these two parameters are strictly correlated: in configurations where only one H_2O or no H_2O are located between the two positively charged units, the MDAP-SERO separation decreases with respect to the minimum energy structure. Conversely, when more H_2Os are positioned between MDAP and SERO, the distance between the two components of the complex increases. Overall, we observed that, in configurations characterized by shorter MDAP-SERO separations (i.e. with zero or one H_2O located between MDAP and SERO), the oscillator strength of the CT bands increases with respect to the minimum energy structure. Hence, a smaller MDAP-SERO separation seems to be a relevant factor for increasing the CT intensity, and water molecules play a key role in fine-tuning the distance between SERO and MDAP. Nonetheless, in the thermally-averaged spectrum of MDAP+SERO complex, the intensity is still lower than the experimental values, suggesting that there are likely other factors, not included in our models, that may affect this quantity. Actually, until now, the host system has not been explicitly considered in the cluster models. Hence, we built new cluster models to investigate the effect of the ZL matrix on the position and intensity of the CT bands. This analysis – reported in Section S7 - was performed on (MDAP)ZL and (MDAP+SERO)ZL minimum energy structures, in order to disentangle the effect of the ZL host from the already discussed thermal effects.

S7. Simulated UV-Vis spectra from cluster models including ZL host

S7.1 (MDAP)ZL

In the case of the cluster model including ZL cut from the minimum energy structure of (MDAP)ZL, 30 excited states were considered in the TD-DFT calculations. The results indicate that the ZL host does not influence significantly MDAP electronic excitations. Fig. S33 shows the comparison of UV-Vis spectra obtained without ZL framework (red line) and with ZL framework (black line). Notably, the inclusion of the ZL framework brings about only modest changes in the electronic spectrum of MDAP. In particular, the two longest-wavelength peaks, associated to the HOMO→LUMO and HOMO→LUMO+1 excitations, undergo only a slight blue-shift and a very small decrease of the intensity. The negligible influence of the ZL environment on the electronic excitation spectra of MDAP can be ascribed to the solvent effect of zeolitic water molecules (which completely surround

the MDAP moiety), thus screening ZL host effects on the electronic transitions of the dye. Such a structural information on the behavior of MDAP in ZL can be gathered by inspecting the g(r) of the MDAP aromatic C atoms with the ZL framework oxygens, which is completely unstructured (see Fig. S28, black line in the top panel).

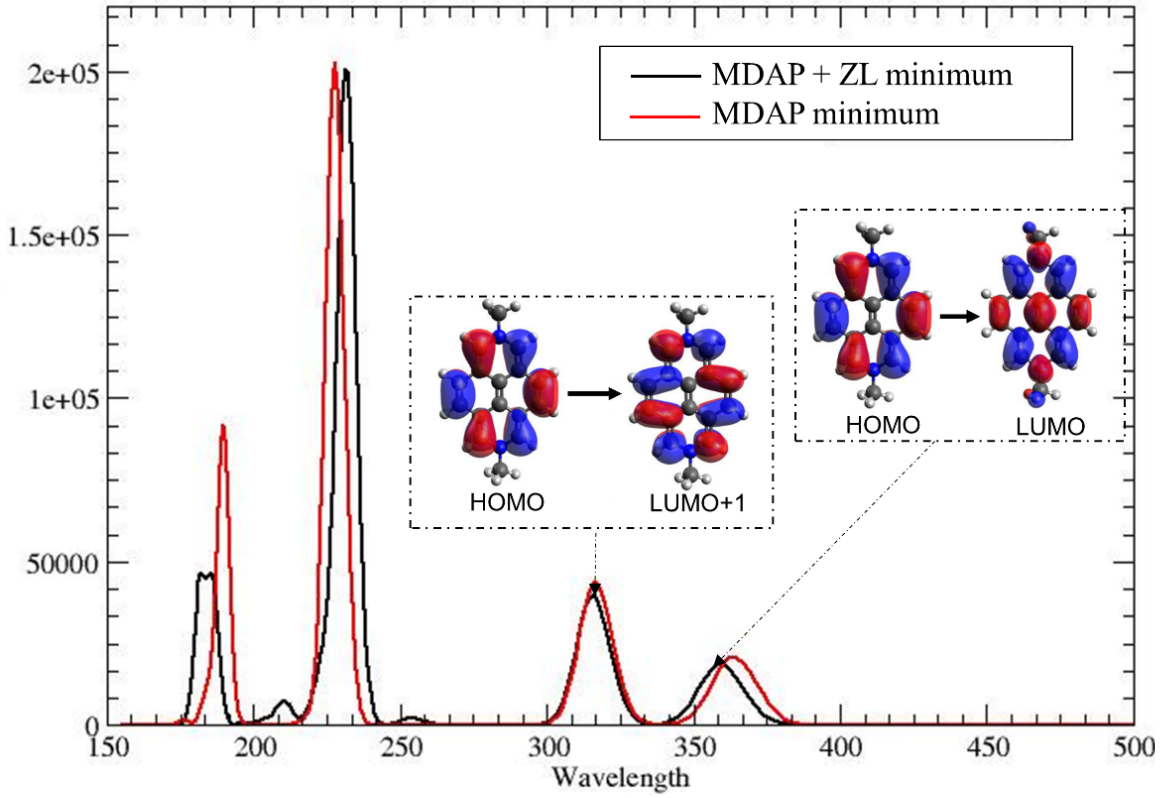

Fig. S33: Comparison of the electronic excitation spectra obtained from cluster models extracted from the minimum energy structure of (MDAP)ZL with inclusion of the ZL framework (black line), and without the ZL framework (red line). The insets illustrate the MOs involved in the two lowest-energy excitations.

S7.2 (MDAP+SERO)ZL

In the case of the cluster model including ZL cut from the minimum energy structure of (MDAP+SERO)ZL, 65 excited states were considered in the TD-DFT calculations. The results indicated that the effect of the ZL framework on the electronic excitations of the complex is much more significant with respect to (MDAP)ZL. The comparison of the electronic excitation spectra of (MDAP+SERO)ZL and (MDAP)ZL (Fig. S34), both computed by including the ZL framework, shows that, in the complex, the signals associatable to the excitations localized only on MDAP are red-shifted. Importantly, in the (MDAP+SERO)ZL spectrum, the CT signals are now clearly identifiable, as a broad band at 457-460 nm, and a shoulder at 395-400 nm. Both CT bands have much higher intensity with respect to what found without ZL framework (see also Fig. S17).

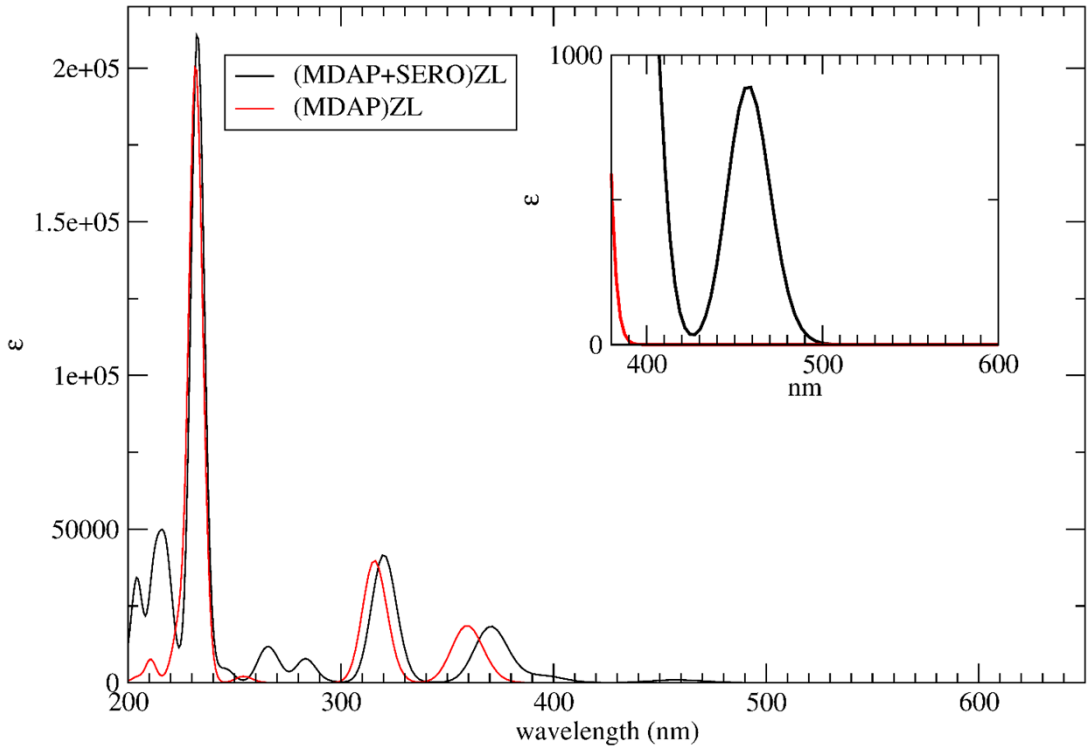

Fig. S34: Comparison of the electronic excitation spectra obtained from cluster models extracted from the minimum energy structures of (MDAP+SERO)ZL (black line), and (MDAP)ZL (red line) with inclusion of the ZL framework. The HOMO→LUMO CT band at 457-460 nm (Table S3) is shown in the inset.

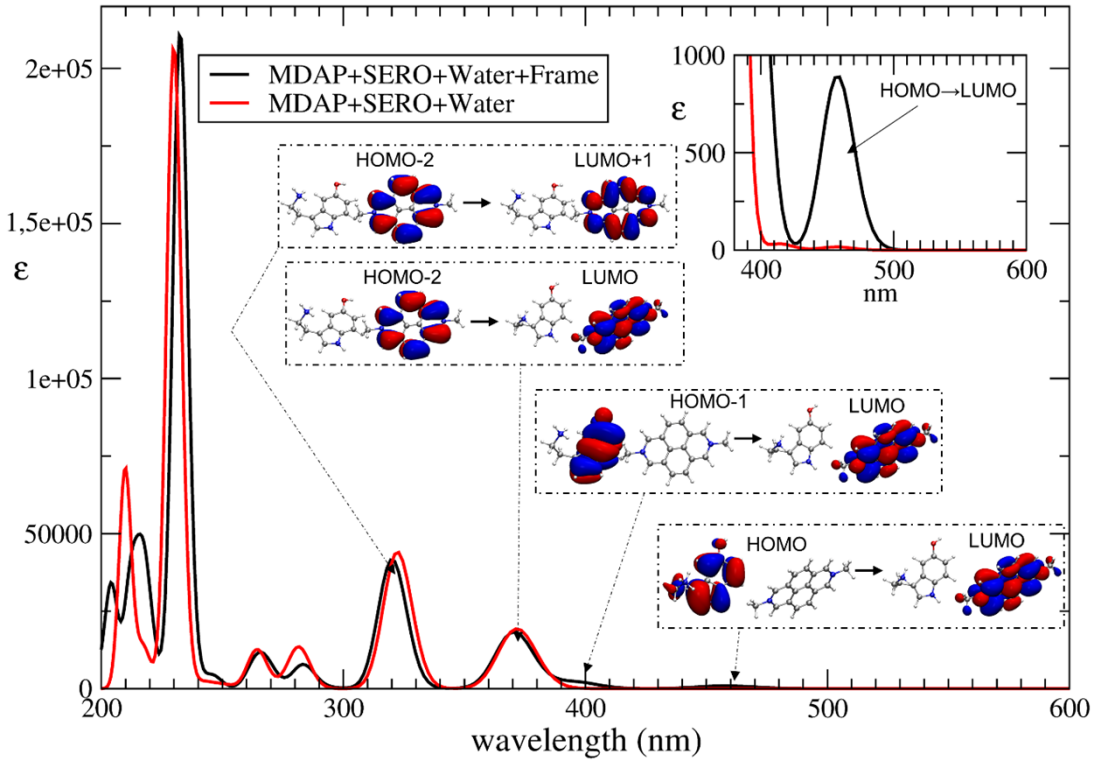

Fig. S35: Comparison of the electronic excitation spectra obtained from cluster models extracted from the minimum energy structure of (MDAP+SERO)ZL with inclusion of the ZL framework (black line), and without the ZL framework (red line). The insets illustrate the MOs involved in the electronic excitations pertaining to the CT bands and to the two highest wavelength bands localized on MDAP.

In Fig. S35, the comparison of the spectrum of (MDAP+SERO)ZL obtained by including the ZL framework in the TD-DFT calculation (black line), with the spectrum computed without the framework (red line) indicates that the inclusion of the ZL framework brings about a significant increase of intensity of the CT bands. In particular, the intensity of the HOMO→LUMO CT band (which was very low in the spectra without the framework) increases by about one order of magnitude (see also Table S3). Conversely, the position of such band is not altered by the ZL environment. Also, the intensity of the HOMO-1→LUMO CT band grows significantly, while its position is blue-shifted (from 414 to 395 nm).

A possible explanation of the greater effect of the ZL environment on the MDAP+SERO complex in comparison to the case of MDAP is that the water molecules do not completely surround the complex, which can get close to the zeolite pore walls. Indeed, as previously mentioned, the SERO unit interacts with ZL via strong hydrogen bonds formed by the protons of the $–NH_3$ and –OH groups with the framework oxygens. Therefore, solvation due to water molecules may not be sufficient to fully screen the MDAP+SERO complex from the effect of the framework atoms**.** Nonetheless, overall the presence of the ZL framework does not appear to alter the MOs shape (see Fig. S36). As already noticed for the orbitals calculated in the absence of the ZL framework, most of the MOs are localized on either MDAP or SERO only (Fig. S36). Indeed, in the simulated UV-Vis spectrum several bands can be ascribed either to MDAP or to SERO as individual components. For example, the 370 nm and 320 nm excitations very closely resemble the HOMO→LUMO and HOMO→LUMO+1 transitions of MDAP without SERO (Fig. S34). Bands associated to excitations localized only on MDAP are also calculated at 232 nm (the most intense peak of the spectrum), at 203 nm and at 188 nm. Both the wavelengths and the shape of the orbitals involved in these transitions (see Table S3 and Fig. S34-S35) are very similar to those obtained without the ZL framework (see Table S2 and Fig. S16-S17). Likewise, bands that can be assigned essentially to SERO excitations are found at 283 and 269 nm, as well as in the 211-218 nm region (see Fig. S35, Table S3, and Fig. S36). Actually, with respect to the spectrum without ZL, the decrease in intensity observed for the 283 nm peak (HOMO→ LUMO+12) may be ascribed to the concomitant growth of the HOMO→ LUMO CT band.

Interestingly, by inspecting the data in Table S3, it emerges that, besides the already discussed HOMO→LUMO and HOMO-1→LUMO CT transitions, there are other charge-transfer excitations which were not present in the spectrum computed without the ZL framework. While the longest-wavelength one, HOMO→LUMO+1 at 400 nm, has a very low oscillator strength, the CT excitations at shorter wavelengths (HOMO→LUMO+5, HOMO→LUMO+9, and HOMO-1→ LUMO+9 at 233-243, 219 and 203 nm, respectively), are characterized by a considerably high oscillator strength.

Hence, such CT transitions contribute significantly to the bands localized in the 200-250 nm region of the electronic excitation spectrum, in which the differences between the spectra calculated with and without the ZL framework become particularly evident (Fig. S35).

Excitation	λ	f
108→109 HOMO→LUMO	**460.41**	**0.0019**
108→109 HOMO→LUMO	**456.34**	**0.0037**
108→110 HOMO→LUMO+1	**400.52**	**0.0002**
107→109 HOMO-1→LUMO	**397.02**	**0.0056**
107→109 HOMO-1→LUMO	**394.24**	**0.0078**
106→109 HOMO-2→LUMO	370.53	0.1131
107→110 HOMO-1→LUMO+1	351.22	0.0000
106→110 HOMO-2→LUMO+1	320.16	0.2575
108→121 HOMO→LUMO+12	283.34	0.0476
107→121 HOMO-1→LUMO+12	269.68	0.0226
107 →114 HOMO→LUMO+5	**243.17**	**0.0018**
107 →114 HOMO→LUMO+5	**233.03**	**0.1352**
101→109 HOMO-7→LUMO	232.66	1.0076
101→110 HOMO-7→LUMO+1	231.32	0.1699
108→118 HOMO→ LUMO+9	**219.35**	**0.0288**
107→120 HOMO-1→ LUMO+11 108→120 HOMO→ LUMO+11 108→121 HOMO→ LUMO+12	217.68	0.1125
108→121 HOMO→ LUMO+12 108→122 HOMO→ LUMO+13 107→122 HOMO-1→ LUMO+13 108→120 HOMO→ LUMO+11	215.74	0.0303
107→121 HOMO-1→ LUMO+12 108→121 HOMO→ LUMO+12 108→129 HOMO→ LUMO+20	212.60	0.1671
107→122 HOMO-1→ LUMO+13 107→121 HOMO-1→ LUMO+12	210.85	0.0401
107→118 HOMO-1→ LUMO+9 107→129 HOMO-1→ LUMO+20	**204.71**	**0.1301**
107→118 HOMO-1→ LUMO+9 107→120 HOMO-1→ LUMO+11	**203.10**	**0.0493**
99→110 HOMO-9→LUMO	202.82	0.0354
103→114 HOMO-5→LUMO+5	188.39	0.4436

Table S3. Assignment of the bands in the simulated UV-Vis spectrum (Fig. S34-S35) of the hydrated MDAP+SERO complex including the ZL framework (see model in Fig. S5a) in terms of MOs (shown in Fig. S36). Green and red colors refer to MOs mostly localized on MDAP and SERO, respectively, while black refers to MOs localized on both moieties. Excitations colored in red and green belong to MDAP and SERO, respectively, as individual units, while the black color refers to CT transitions. For higher-energy bands, only the main component(s) of the transitions have been included in Table S3.

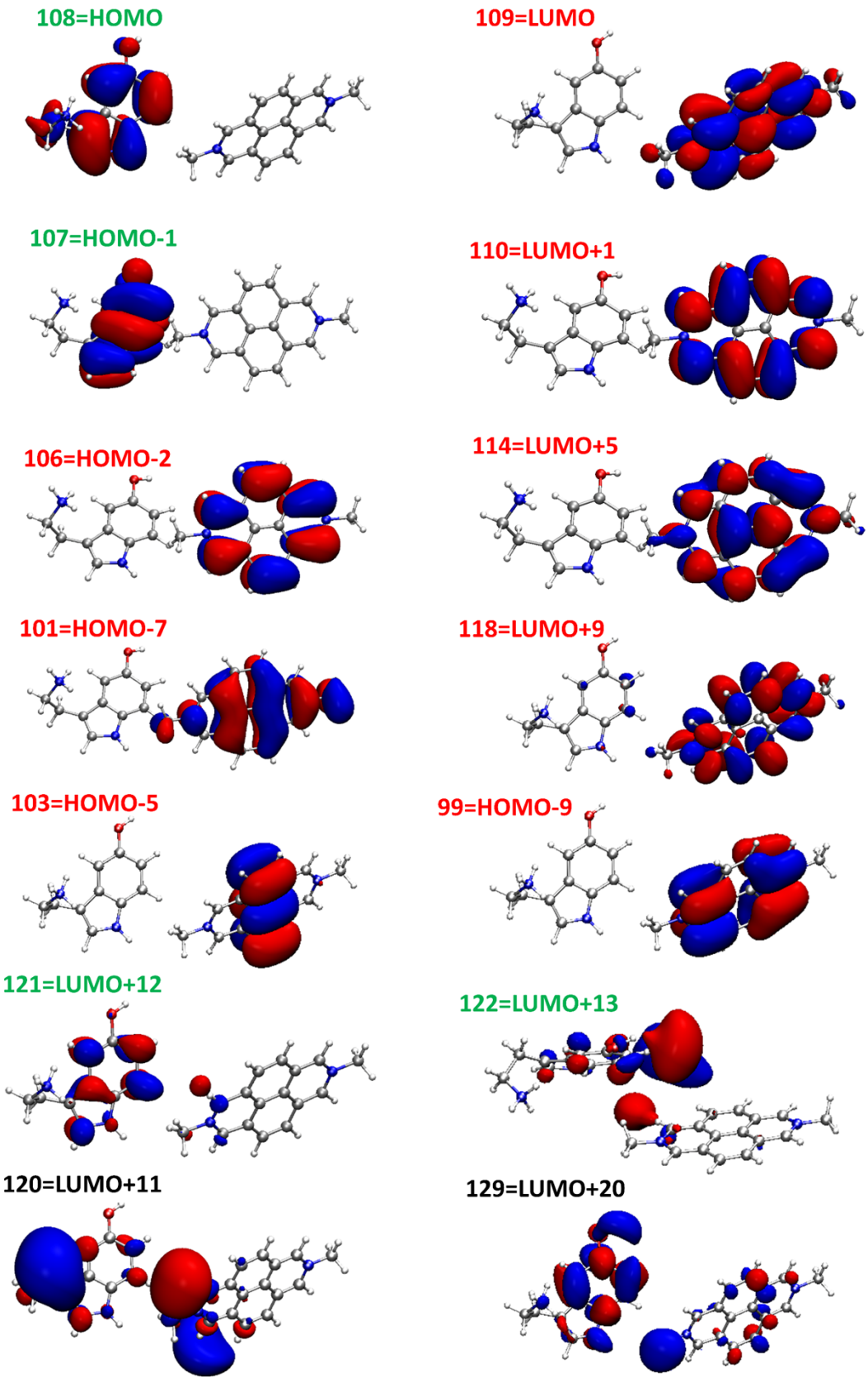

Fig. S36. Molecular orbitals of the MDAP+SERO complex involved in the electronic excitations computed by including also a point-charge model of the ZL framework in the TD-DFT calculations, and reported in Table S3. MOs localized on MDAP and on SERO are labeled in red and green, respectively. MOs delocalized on both MDAP and SERO moietes are labeled in black.

Overall, the present comparison of the electronic excitation spectra of the MDAP+SERO complex computed with and without the ZL framework has highlighted a crucial role of the ZL host in enhancing the CT excitations of the complex in the entire UV-vis range. In particular, thanks to the interactions of the MDAP+SERO complex with the zeolite host, the intensity of the HOMO→LUMO and HOMO-1→LUMO CT excitations increases by at least one order of magnitude. More specifically, this intensity increase could be ascribed to the fact that the electron density donor – the positively charged SERO – is located close to the ZL channel walls, forming strong hydrogen bonds with negatively charged AlO_4 tetrahedral units. Hence, such an interaction may enhance the SERO propensity to transfer electronic density to a close electron acceptor – i.e. the MDAP dication, causing an increase of intensity of charge-transfer excitations.

Importantly, the two above-mentioned CT bands are responsible of the high-wavelength tail detected in the optical spectra of (MDAP)ZL upon titration with SERO.[4] Hence, it can be concluded that host-guest interactions – in particular, the direct connection of SERO with the ZL framework via hydrogen-bonding - play a key role in the sensing mechanism of nanozeolite receptors, being at the origin not only of the high binding specificity, but also of the exceptional sensitivity experimentally detected for this system.[4] This insight might be exploited to further improve nanozeolite receptors by optimizing the combination between the zeolite host and the reporter dye as a function of the analyte. Indeed, besides the formation of a confined complex between analyte and dye – which should be close enough to enable CT, strong interactions of the analyte with the host are particularly relevant for maximizing the intensity of the CT signal.

S8. Description of the "MDAP_SERO_ZL.mpeg" movie.

The "MDAP_SERO_ZL.mpeg" movie, sketching the room-temperature dynamical behavior of the (MDAP+SERO)ZL system, has been realized using the AIMD trajectory collected for the (MDAP+SERO)ZL periodic model.

For simplicity, the ZL framework oxygen atoms were not explicitly represented in the "MDAP_SERO_ZL.mpeg" movie. The structure of the ZL framework is shown as a yellow stick model, while the extraframework K^+ cations are represented as violet spheres. For the guest species, color codes are as follows: cyan=C; blue=N; red=O; white=H. Hydrogen bonds are shown as dashed lines.

In the "MDAP_SERO_ZL.mpeg" movie, two simulation cells of the (MDAP+SERO)ZL periodic model are visualized. The intermolecular complex considered in the calculations of the present work is the one constituted by the closest MDAP+SERO pair. Hence, in the "MDAP_SERO_ZL.mpeg"

movie, two replicas of the MDAP+SERO intermolecular complex are shown. Their shortest distance amounts to 5.6 Å in the minimum energy structure, and oscillates only slightly around this value along the AIMD simulation. As demonstrated in paragraph S4.4, such a value of the separation among the replicas is sufficient to ensure that the contribution of periodically repeated images to the CT bands in the electronic excitation spectra is negligible.

The visualization of two simulation cells along the *z* axis allows one to appreciate the presence of a dense layer of zeolitic water molecules separating the two replicas of the MDAP+SERO intermolecular complex.

REFERENCES

1 Ch. Baerlocher, L. B. McCusker and D. H. Olson, *Atlas of Zeolite framework types*, Published on behalf of the Structure Commission of the International Zeolite Association by Elsevier, 2007.
2 R. M. Barrer and H. Villiger, *Zeitschrift für Kristallographie - Crystalline Materials*, 1969, **128**, 352–370.
3 G. Calzaferri, R. Méallet-Renault, D. Brühwiler, R. Pansu, I. Dolamic, T. Dienel, P. Adler, H. Li and A. Kunzmann, *ChemPhysChem*, 2011, **12**, 580–594.
4 L. M. Grimm, S. Sinn, M. Krstić, E. D'Este, I. Sonntag, E. A. Prasetyanto, T. Kuner, W. Wenzel, L. De Cola and F. Biedermann, *Adv. Mater.*, 2021, **33**, 2104614.
5 J. M. Newsam, *The Journal of Physical Chemistry*, 1989, **93**, 7689–7694.
6 L. Gigli, G. Vezzalini, S. Quartieri and R. Arletti, *Microporous and Mesoporous Materials*, 2019, **276**, 160–166.
7 D. J. Frisch, M. J.; Trucks, G. W.; Schlegel, H. B.; Scuseria, G. E.; Robb, M. A.; Cheeseman, J. R.; Scalmani, G.; Barone, V.; Mennucci, B.; Petersson, G. A.; Nakatsuji, H.; Caricato, M.; Li, X.; Hratchian, H. P.; Izmaylov, A. F.; Bloino, J.; Zheng, G.; Sonnenb, Gaussian 09, Revision E.01, Gaussian, Inc., Wallingford CT 2009.
8 J. P. Perdew, K. Burke and M. Ernzerhof, *Phys. Rev. Lett.*, 1996, **77**, 3865–3868.
9 S. Grimme, *J. Comput. Chem.*, 2006, **27**, 1787–1799.
10 D. Vanderbilt, *Phys. Rev. B*, 1990, **41**, 7892–7895.
11 K. F. Garrity, J. W. Bennett, K. M. Rabe and D. Vanderbilt, *Comput. Mater. Sci.*, 2014, **81**, 446–452.
12 L. Kleinman and D. M. Bylander, *Physical Review Letters*, 1982, **48**, 1425–1428.
13 N. Troullier and J. L. Martins, *Physical Review B*, 1991, **43**, 1993–2006.
14 D. Hamann, M. Schlüter and C. Chiang, *Physical Review Letters*, 1979, **43**, 1494–1497.
15 S. Nosé, *The Journal of Chemical Physics*, 1984, **81**, 511–519.
16 W. G. Hoover, *Physical Review A*, 1985, **31**, 1695–1697.
17 R. Car and M. Parrinello, *Physical Review Letters*, 1985, **55**, 2471–2474.
18 D. Marx and J. Hutter, *Ab Initio Molecular Dynamics*, Cambridge University Press, Cambridge, 2009.
19 IBM Corp. 1990–2017 and MPI für Festkörperforschung Stuttgart 1997–2001, CPMD: Car Parrinello Molecular Dynamics http://www.cpmd.org 2017.
20 J.-D. Chai and M. Head-Gordon, *Physical Chemistry Chemical Physics*, 2008, **10**, 6615.
21 C. Adamo and V. Barone, *The Journal of Chemical Physics*, 1999, **110**, 6158–6170.

22 E. Fois, G. Tabacchi and G. Calzaferri, *Journal of Physical Chemistry C*, 2012, **116**, 16784–16799.
23 E. Fois, G. Tabacchi, A. Devaux, P. Belser, D. Brühwiler and G. Calzaferri, *Langmuir*, 2013, **29**, 9188–9198.
24 M. Caricato, G. W. Trucks, M. J. Frisch and K. B. Wiberg, *J. Chem. Theory Comput.*, 2011, **7**, 456–466.
25 M. E. Casida, C. Jamorski, K. C. Casida and D. R. Salahub, *J. Chem. Phys.*, 1998, **108**, 4439–4449.
26 T. Yanai, D. P. Tew and N. C. Handy, *Chem. Phys. Lett.*, 2004, **393**, 51–57.
27 R. J. Woods and R. Chappelle, *J. Mol. Struc. THEOCHEM*, 2000, **527**, 149–156.
28 J. Kuhn, J. M. Castillo-Sanchez, J. Gascon, S. Calero, D. Dubbeldam, T. J. H. Vlugt, F. Kapteijn and J. Gross, *J. Phys. Chem. C*, 2009, **113**, 14290–14301.
29 C. Cabezas, M. Varela, I. Peña, J. C. López and J. L. Alonso, *Phys. Chem. Chem. Phys.*, 2012, **14**, 13618–13623.
30 A. Klamt and G. Schüürmann, *Journal of the Chemical Society, Perkin Transactions 2*, 1993, **0**, 799–805.
31 J. Tomasi, B. Mennucci and R. Cammi, *Chemical reviews*, 2005, **105**, 2999–3094.